



An-Najah National University
Faculty of Graduate Studies

**STRUCTURAL, ELECTRONIC, ELASTIC
AND MAGNETIC PROPERTIES OF THE
CeXO₃(X=Cr, Ga) COMPOUNDS BY USING
FP-LAPW METHOD**

By

Omar Rustum Mushref Kabi

Supervisor

**Prof. Mohammed Abu-Jafar
Dr. Mahmoud Farout**

**This Thesis is submitted in Partial Fulfillment of the Requirements for the Degree
of Master of physics, Faculty of Graduate Studies, An-Najah National University,
Nablus, Palestine.**

2022

**STRUCTURAL, ELECTRONIC, ELASTIC
AND MAGNETIC PROPERTIES OF THE
CeXO₃(X=Cr, Ga) COMPOUNDS BY USING
FP-LAPW METHOD**

By

Omar Rustum Mushref Kabi

This Thesis was Defended Successfully on 29/05/2022 and approved by

Prof. Mohammed Abu-Jafar
Supervisor

Signature

Dr. Mahmoud Farout
Co-Supervisor

Signature

Dr. Abdel-Rahman Abu-Lebdeh
External Examiner

Signature

Prof. Mohammed Elsaid
Internal Examiner

Signature

Dedication

I offer this work to my family who shared with me all the moments and helped me to overcome all obstacles, to my mother who did everything for me, to my father - may God have mercy on him - who was and still is with me in his spirit and in every step I take in my life, to Professor Issam Al-Ashqar - May God have mercy on him - from whom we learned the meanings of sincerity and morals before education.

Acknowledgments

First of all, I always thank God for making me pass this message successfully. I would like to thank my doctors, teachers and supervisors, Prof. Dr. Mohammad Abu-Jafar, for all he did for me to end this phase of help, discussion, guidance and encouragement. I also thank my Co-supervisor, Dr. Mahmoud Farout for everything he did to help me complete this project; from practice until the end of this work. I am proud that you are my supervisors. I do not forget the faculty members for their constant assistance to me.

Declaration

I, the undersigned, declare that I submitted the thesis entitled:

STRUCTURAL, ELECTRONIC, ELASTIC AND MAGNETIC PROPERTIES OF THE CeXO_3 ($\text{X}=\text{Cr}, \text{Ga}$) COMPOUNDS BY USING FP-LAPW METHOD

I declare that the work provided in this thesis, unless otherwise referenced, is the researcher's own work, and has not been submitted elsewhere for any other degree or qualification.

Student's Name:

Omar Rustum Mushref Kabi

Signature:

Date:

29/05/2022

Table of contents

Dedication.....	III
Acknowledgments	IV
Declaration.....	V
Table of contents.....	VI
List of Tables	VII
List of Figures.....	VIII
List of Appendices	X
Abstract	XI
Chapter One: Introduction	1
Chapter Two: Methodology.....	4
2.1 The Open-Heimer Approximation:.....	4
2.2 Hartree and Hartree-Fock Approximation:	5
2.3 Density Functional Theory	5
2.4 Single Particle Kohn-Sham Equation	6
2.5 The Exchange-Correlation Functional	8
2.6 Local Density Approximation (LDA).....	8
2.7 Generalized Gradient Approximation (GGA)	8
2.8 The Modified Becke-Johnson (mBJ) potential	9
2.9 Augmented Plane Wave (APW) Method.....	9
2.10 The Linearized Augmented Plane Wave (LAPW) Method.....	10
2.11 WIEN2k code	11
Chapter Three: Computational method.....	12
Chapter Four: Results and Discussion	13
4.1 Structural properties.....	13
4.2 Electronic properties.....	19
4.3 Magnetic Properties.....	24
4.4 Elastic properties.....	26
Chapter 5: Conclusions.....	29
References.....	30
Appendices.....	34
الملخص.....	ب

List of Tables

Table (1): Calculated lattice parameter, bulk modulus, pressure derivative of CeCrO ₃ in a cubic structure	14
Table (2): Calculated lattice parameter, bulk modulus, pressure derivative of CeCrO ₃ in orthorhombic structure.....	15
Table (3): Calculated lattice parameter, bulk modulus, pressure derivative of CeGaO ₃ in a cubic structure.....	17
Table (4): Calculated lattice parameter, bulk modulus, pressure derivative of CeGaO ₃ in orthorhombic structure.....	18
Table (5): Energy band gap (E _g) of CeCrO ₃ and CeGaO ₃ compounds using PBE-GGA methods.....	20
Table (6): The total magnetic moment for Cubic and Orthorhombic CeCrO ₃ compound using PBE-GGA method.	25
Table (7): The total magnetic moment for Cubic and Orthorhombic CeCrO ₃ compounds with mBJ-GGA potential.....	25
Table (8): The total magnetic moment for Cubic and Orthorhombic CeGaO ₃ compounds by using PBE-GGA method	26
Table (9): The total magnetic moment for Cubic and Orthorhombic CeGaO ₃ compounds with mBJ-GGA potential.....	26
Table (10): Calculated elastic constants of CeCrO ₃ and CeGaO ₃ in the cubic structure	28
Table (11): Calculated elastic constants of CeCrO ₃ and CeGaO ₃ in the orthorhombic structure	34

List of Figures

Figure (1): Ideal cubic perovskite structure (ABO ₃).....	2
Figure (2): Flow chart for the <i>nth</i> iteration in the self-consistent procedure to solve Hartree-Fock or Kohn-Sham equations.	7
Figure (3): scheme of Augmented Plane Wave.....	10
Figure (4): Equation of state of cubic perovskite of CeCrO ₃ PBE-GGA methods, (EvsV).....	14
Figure (5): Equation of state of orthorhombic perovskite of CeCrO ₃ PBE-GGA methods, (E vs V).	15
Figure (6): The relationship between Equation of state of the Cubic and orthorhombic perovskite of CeCrO ₃ PBE-GGA methods, (E vs V).....	16
Figure (7): Equation of state of cubic perovskite of CeCrO ₃ PBE-GGA methods, (EvsV).....	17
Figure. (8): Equation of state of orthorhombic perovskite of CeGaO ₃ PBE-GGA methods, (E vs V)	18
Figure (9): The relationship between Equation of state of the Cubic and orthorhombic perovskite of CeGaO ₃ PBE-GGA methods, (E vs V).	19
Figure (10): The Calculated spin polarized (a) up (b) down band structures for cubic CeCrO ₃ compound using PBE-GGA.	21
Figure (11): The Calculated spin polarized (a) up (b) down band structures for cubic CeCrO ₃ compound with mBJ-GGA potential.....	35
Figure (12): The Calculated spin polarized (a) up (b) down band structures for orthorhombic CeCrO ₃ compound using PBE-GGA	36
Figure (13): The Calculated spin polarized (a) up (b) down band structures for orthorhombic CeCrO ₃ compound with mBJ-GGA potential.....	37
Figure (14): The Calculated spin polarized (a) up (b) down band structures for cubic CeGaO ₃ compound using PBE-GGA.....	38
Figure (15): The Calculated spin polarized (a) up (b) down band structures for cubic CeGaO ₃ compound with mBJ-GGA potential.	39
Figure (16): The Calculated spin polarized (a) up (b) down band structures for orthorhombic CeGaO ₃ compound using PBE-GGA.....	40
Figure (17): The Calculated spin polarized (a) up (b) down band structures for orthorhombic CeGaO ₃ compound with mBJ-GGA potential.	41
Figure (18): Total and partial density of state of spin up for (a) CeCrO ₃ , (b) Ce , (c) Cr and (d) O of cubic CeCrO ₃ compound by using PBE-GGA method.....	42
Figure (19): Total and partial density of state of spin down for (a) CeCrO ₃ , (b) Ce , (c) Cr and (d) O of cubic CeCrO ₃ compound by using PBE-GGA method.....	43
Figure (20): Total and partial density of state of spin up for (a) CeCrO ₃ , (b) Ce , (c) Cr and (d) O of cubic CeCrO ₃ compound with mBJ-GGA potential.	44

Figure (21): Total and partial density of state of spin down for (a) CeCrO ₃ , (b) Ce, (c) Cr and (d) O of cubic CeCrO ₃ compound with mBJ-GGA potential.	45
Figure (22): Total and partial density of state of spin up for (a) CeCrO ₃ , (b) Ce, (c) Cr and (d) O of orthorhombic CeCrO ₃ compound by using PBE-GGA.....	46
Figure (23): Total and partial density of state of spin down for (a) CeCrO ₃ , (b) Ce, (c) Cr and (d)O of orthorhombic CeCrO ₃ compound by using PBE-GGA.....	47
Figure (24): Total and partial density of state of spin up for (a) CeCrO ₃ , (b) Ce, (c) Cr and (d) O of orthorhombic CeCrO ₃ compound with mBJ-GGA potential.	48
Figure (25): Total and partial density of state of spin down for (a) CeCrO ₃ , (b) Ce, (c) Cr and (d) O of orthorhombic CeCrO ₃ compound with mBJ-GGA potential.	49
Figure (26): Total and partial density of state of spin up for (a) CeGaO ₃ , (b) Ce, (c) Ga and (d) O of cubic CeGaO ₃ compound by using PBE-GGA method.	50
Figure (27): Total and partial density of state of spin down for (a) CeGaO ₃ , (b) Ce, (c) Ga and (d) O of cubic CeGaO ₃ compound by using PBE-GGA method.....	51
Figure (28): Total and partial density of state of spin up for (a) CeGaO ₃ , (b) Ga, (c) Cr and (d) O of cubic CeGaO ₃ compound with mBJ-GGA potential.....	52
Figure. (29): Total and partial density of state of spin down for (a) CeGaO ₃ , (b) Ga, (c) Cr and (d) O of cubic CeGaO ₃ compound with mBJ-GGA potential.....	53
Figure (30): Total and partial density of state of spin up for (a) CeGaO ₃ , (b) Ce, (c) Ga and (d) O of orthorhombic CeGaO ₃ compound by using PBE-GGA.	54
Figure (31): Total and partial density of state of spin down for (a) CeGaO ₃ , (b) Ce, (c) Ga and (d) O of orthorhombic CeGaO ₃ compound by using PBE-GGA.	55
Figure (32): Total and partial density of state of spin up for (a) CeGaO ₃ , (b) Ce, (c) Ga and (d) O of orthorhombic CeGaO ₃ compound with mBJ-GGA potential.....	56
Figure (33): Total and partial density of state of spin down for (a) CeGaO ₃ , (b) Ce, (c) Ga and (d) O of orthorhombic CeGaO ₃ compound with mBJ-GGA potential.	57

List of Appendices

Appendix (A): Tables	34
Appendix (B): Figures	35

STRUCTURAL, ELECTRONIC, ELASTIC AND MAGNETIC PROPERTIES OF THE CeXO_3 ($\text{X}=\text{Cr, Ga}$) COMPOUNDS BY USING FP-LAPW METHOD

By
Omar Rustum Mushref Kabi
Supervisor
Prof. Mohammed Abu-Jafar
Dr. Mahmoud Farout

Abstract

Background: the full potential linearized augmented plane wave (FP-LAPW) method was used to calculate the structural, electronic, magnetic and elastic properties of cubic and orthorhombic perovskite compounds CeCrO_3 , CeGaO_3 .

Objectives: the FP-LAPW method solves structural parameters (lattice parameters, bulk modulus, and first pressure derivatives of bulk modulus) by solving the Kohn-Sham equations for the total energy of many electron-systems.

Methodology: the structural parameters and the consequent electronic, magnetic and elastic properties were calculated using the generalized gradient approximation (GGA) that determines the density and density gradient.

Results: by examining the energy band gap of these compounds using the modified Becki-Johnson potential (mBJ), we show that the compound CeCrO_3 behaves as a half-metallic behavior in the cubic structure and also half-metallic in orthorhombic structure, and that the CeGaO_3 compound behaves as a semiconductor in cubic structure and it was found that it is a semiconductor in a spin-up state and an insulator in a spin-down state in orthorhombic structure. At the same point, the total magnetic moments were examined, and they were in good agreement with the experimental and theoretical results for these perovskite compounds. The electronic properties of these compounds, which are band structure and density of state, were also calculated. Finally, the elastic properties of these perovskite compounds were studied.

Keywords: FP-LAPW study, perovskite, Half-metallic ferromagnetic, Structural properties, Electronic properties, Magnetic properties, Elastic properties.

Chapter One

Introduction

Perovskite is named after the discovery of these materials in 1792 by Lev Perevsky (1792-1856)^[1]. It is a black or brown mineral with the chemical formula CaTiO_3 and the name of this mineral is calcium titanium oxide discovered by Gustav Rose in the mountains of Russia. In 1926, its crystal was first described^[2] and published for the first time in 1945^[3].

Perovskite compounds have a major formula, ABX_3 . A and B are cations of different masses, where A is greater than B^[4]. X is often to be oxygen or possibly other large ions such as nitrides, sulfides, and halides. It is known that many oxide compounds belong to few homogeneous chains based on perovskite^[5].

In its ideal form, perovskite oxides are cuboidal or somewhat cuboidal in structure like other transition metal oxides that have the same formula (ABO_3). At low temperatures, some phase change may occur. Because of their exceptional crystal structures and simple in their electrical and ferroelectric properties, oxides of compounds have a wide potential for many uses.

Perovskite materials are of three types, the first type has local electrons, the second contains undefined energy band electrons, and the third state is transitional between these two types^[3]. Types of perovskite structures exist in many forms including ABO_3 -perovskite and the most abundant in nature is MgSiO_3 and FeSiO_3 .

Scientists have studied perovskite oxides in solid state physics because of the great importance of these compounds in different topics of physics such as Materials science, astrophysics, fusion, geophysics, particle accelerators, fission reactors^[6,7].

The oxides are considered to be perovskite which has comprehensive properties such as; The properties of ionic conductivity, insulator-to-metal transition and change of solid states phenomena, superconductivity and metallic characters, and finally can be applied in many fields of chemistry and physics^[8].

There are great alternatives to perovskite oxides that can accept one or both of the two existing sites (A and B sites) and their original crystal structures^[9] will be preserved.

Currently, perovskite ceramics have many applications such as transformers, sensors, microwave screens ^[10], piezoelectric devices, ^[11] and random-access memory drives^[12].

Perovskite is used in many modern applications because it has many useful properties in electromechanical, image storage, surface acoustic wave signal, switching, filtering and photochromic ^[13]. Currently, perovskite halide enters into many fields, the most important of which is the exploration of materials^[12] because it has great effectiveness in solid-state solar energy.

The structure of perovskite is often cubic. It consists of A atoms that are at the corners of the cube, B atoms are located in its center in a 6-fold coordination, and it is surrounded by a solid of eight ions, while oxygen atoms are in the centers of the faces. The A cation is in 12 times the cubic octahedral coordination as in Figure 1.

Figure. (1):

Ideal cubic perovskite structure (ABO₃).

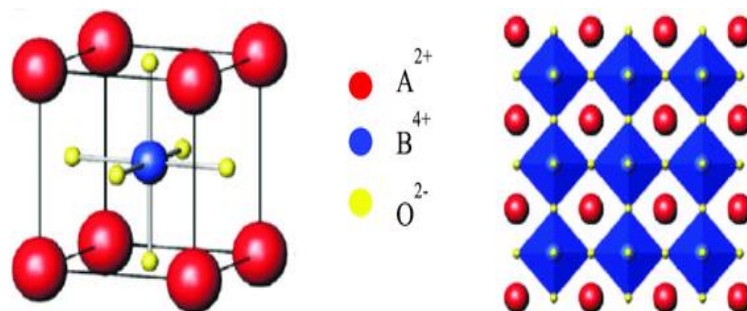


Figure 1 shows a cubic perovskite, the A atom in one cell being a lanthanide ion or an alkaline earth metal ^[14]. In fact, A are cations that are 12 times coordinated by oxygen anions and are present in the corners of the cube at position (0, 0, 0), while the oxygen is located in the center of the face of the cubic lattice at position (1/2, 1/2, 0), but there are inside oxygen. The octahedral cations are B tetravalent and their position is the center of the body (1/2, 1/2, 1/2). This structure is a three-dimensional network imaged from the angle associated with the angle BO₆ octahedron ^[15].

Perovskite contains a large number of compounds, its structure is very stable, it has a variety of applications, and it also has different properties. The most important role of octahedral BO₆ is in ferroelectricity and ferromagnetism. Material optimization comes from the broad composition of solid solutions by controlling the geometry of the phase

transition and the control of the structure ^[16]. Figure 1 also shows the single-cell structure of a simple perovskite.

There may be several changes in the shape of the perfect cubic perovskite and this result in the formation of hexagonal, orthorhombic, rhombohedral, and tetrahedral shapes. In general, to form a perovskite, we have to meet two requirements which are the requirements for ionic radii and electron neutrality ^{[17][18]}.

The (FP-LAPW) method will be used in this work to examine the following structural, electronic, magnetic and finally elastic properties of the two perovskite compounds CeCrO₃, CeGaO₃.

Chapter Two

Methodology

It is difficult for us to solve Schrödinger equation for the N-body system, equation (1), so we must use some approximations to deal with many body problems ^[19, 20]. Schrödinger equation begins with the Hamiltonian operator given by:

$$\hat{H} = -\frac{\hbar^2}{2} \sum_{i=1}^N \frac{\nabla_{\vec{R}_i}^2}{M_i} - \frac{\hbar^2}{2} \sum_{i=1}^N \frac{\nabla_{\vec{r}_i}^2}{m_e} - \frac{1}{4\pi\epsilon_0} \sum_{ij} \frac{e^2 Z_i Z_j}{|\vec{R}_i - \vec{r}_j|} + \frac{1}{8\pi\epsilon_0} \sum_{i \neq j} \frac{e^2}{|\vec{r}_i - \vec{r}_j|} + \frac{1}{8\pi\epsilon_0} \sum_{i \neq j} \frac{e^2 Z_i Z_j}{|\vec{R}_i - \vec{R}_j|} \quad (1)$$

In this equation, the kinetic energy operator of the nucleus (T_n) is the first term, while the second term is for electrons (T_e). The last three terms in this equation are in the following order; the electric attraction between the electrons and the nuclei (V_{en}), the electric repulsion between electrons (V_{ee}), and the electric repulsion between nuclei (V_{nn}).

This equation does not have an exact solution. Therefore, we must use some approximations to simplify its solution, and these approximations are:

2.1 The Open-Heimer Approximation:

This approximation is used to simplify the interaction between nuclei and electrons ^[21,22]. It assumes that the movement of the heavier nucleus adapts to the lighter electrons and is in their instantaneous ground state ^[23] at any time. This approximation neglects the motion of the nuclei when comparing it with the electron because the nuclei are heavy masses relative to electrons, therefore, have zero kinetic energy. This means that the first term in Schrödinger equation can be neglected and the last term will be considered as a constant ^[19]. Therefore, equation (1) will be reduced to the following form:

$$H = T_e + V_{ee} + V_{ext} \quad (2)$$

In this equation, T_e is an abbreviation for the kinetic energy of electron gas, the potential energy for electron-electron interactions is V_{ee} , and finally V_{ext} is the external potential, which is $V_{ext} = V_{nn} + V_{en}$

2.2 Hartree and Hartree-Fock Approximation:

No two electrons can have the same set of quantum numbers. This is the Pauli exclusion principle and this is what is considered in the Hartree approximation [24]. The Hartree-Fock approximation assumes that the electrons are independent of each other, so the Hamiltonian can be considered as N-one particle Hamiltonian. The wave function of the electrons is given as follows:

$$\Psi(\vec{r}_1, \vec{r}_2, \vec{r}_3, \dots, \vec{r}_N) = \Psi_1(\vec{r}_1) \Psi_2(\vec{r}_2) \Psi_3(\vec{r}_3) \dots \Psi_N(\vec{r}_N) \quad (3)$$

In this equation, $\Psi_N(\vec{r}_N)$ is a wave function of the Nth electron. Schrodinger equation is given as:

$$(T_s + V_{ext} + V_H) \Psi(\vec{r}) = E \Psi(\vec{r}) \quad (4)$$

T_s is the kinetic energy, V_{ext} is the external potential and V_H is the Hartree potential for non-interacting electrons. We can write the V_H equation as follows:

$$V_H = \frac{1}{8\pi\epsilon_0} \sum_{ij}^N \frac{|\psi(\vec{r}_i)|^2 |\psi(\vec{r}_j)|^2 d^3r_i d^3r_j}{|\vec{r}_i - \vec{r}_j|} \quad (5)$$

2.3 Density Functional Theory

The density functional theory was established in 1964 by the theories of Hohenberg and Kohn. It can be said that the density functional theory replaces the electron wave function of many objects with the electron density [25, 26] and this theory is more powerful and modern than the Hartree-Fock approximation. DFT is used to solve the many-body problem in a one-body problem.

The DFT theory is based on both Kohn and Hohenberg theories [19]. The 3N Schrödinger equation can be reduced to 3 spatial coordinates by both theorems. The first theory says that the density of the ground state (ρ_0) will be produced by the successful reduction of the energy function. While the second theory defines the electron wave theory and thus determines all the ground state properties of an electronic system by the ground state electron density [27]. To solve the variance problem to reduce the energy function $E(\rho)$, the lagrangian application of indeterminate multiples can be used. For this we will rewrite $E(\rho)$ as the total Hartree energy plus another unknown function called the exchange correlation function $E_{xc}(\rho)$.

$$E(\rho) = T_s(\rho) + E_c(\rho) + E_H(\rho) + E_{ii}(\rho) + E_{xc}(\rho) \quad (6)$$

In this equation, we used the symbol \mathbf{T}_s to refer to a single electronic kinetic energy, and we refer to the Coulomb energy between nuclei and electrons with the symbol \mathbf{E}_c , while $\mathbf{E}_{ii}(\rho)$ to denote the interaction between the nuclei, \mathbf{E}_{xc} is the exchange correlation energy of an unknown part, and finally \mathbf{E}_H is the Hartree potential energy which is defined by the following equation:

$$E_H(\rho) = \frac{e^2}{2} \int d^3 r \int d^3 r' \frac{\rho(\vec{r})\rho(\vec{r}')}{|\vec{r} - \vec{r}'|} \quad (7)$$

Schrödinger equation for one electron can be written as follows:

$$[T_s + V_{ext}(r) + V_H(\rho(r)) + V_{XC}(\rho(r))] \Phi_i(r) = \varepsilon_i \Phi_i(r) \quad (8)$$

In this equation, ε_i is the single particle energy, φ_i is the electron wave function, V_H is the Hartree potential, V_{ext} is the coulomb potential and V_{XC} is the exchange-correlation potential.

2.4 Single Particle Kohn-Sham Equation

We solve the Kohn-Sham equations of the ground state density, Eigen values and the total energy for a multi-electron system using the LAPW method^[19].

It can be said that it undergoes two external potential; the first is due to the nuclei $\widehat{V}_{ext}[\rho]$, and the second is due to the exchange and correlation effect $\widehat{V}_{xc}[\rho]$, which is an energy functional for a classical unreacted electron gas. Where the exact ground-state density $\rho(r)$ of an N-electron system is defined as:

$$\rho(\vec{r}) = \sum_{i=1}^N \phi_i^*(\vec{r})\phi_i(\vec{r}) = \sum_{i=1}^N |\phi_i(\vec{r})|^2 \quad (9)$$

where $\phi_i(\vec{r})$ is a one-particle wave function, which is the N lowest-energy solution of the Kohn- Sham equation. This equation can be written by:

$$\widehat{H}_{KS}\phi_i = \varepsilon_i\phi_i \quad (10)$$

The Kohn-Sham equation can be written in another form as follows:

$$\widehat{H}\phi_i(\vec{r}) = \left[-\frac{\hbar^2}{2m_e} \nabla_i^2 + V_{eff} \right] \phi_i = \varepsilon_i\phi_i \quad (11)$$

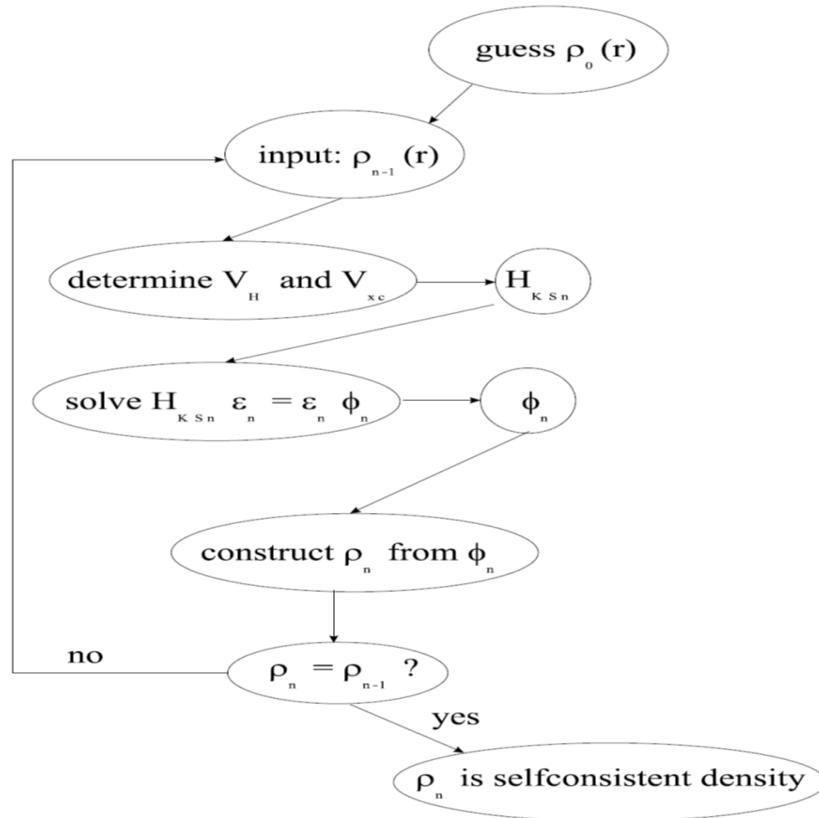
where \hat{H} is the Hamiltonian operator, while \mathbf{V}_{eff} is the effective potential and it is the sum of the external voltage, the exchange-correlation potential and the Hartree potential and is given in equation (12):

$$V_{\text{eff}}(\vec{r}) = V_{\text{ext}}(\vec{r}) + \frac{\delta E_{\text{H}}[\rho]}{\delta \rho} + \frac{\delta E_{\text{xc}}[\rho]}{\delta \rho} = V_{\text{ext}}(\vec{r}) + \frac{e^2}{4\pi\epsilon_0} \int \frac{\rho(\vec{r}')}{|\vec{r}-\vec{r}'|} d\vec{r}' + V_{\text{xc}}(\vec{r}) \quad (12)$$

We conclude from the previous equation that \mathbf{V}_{H} and \mathbf{V}_{xc} depend on the charge density $\rho(\vec{r})$, and can be calculated from ϕ_i . This means that we are dealing with self-consistency problems: it shows us the original equation (V_{H} and V_{xc} in H_{KS}), and it is very difficult to write down the equation and solve it before knowing its solution. Some starting density ρ_0 is guessed, and a Hamiltonian $H_{\text{KS}1}$ can be constructed with it. The Eigen value problem is solved, and ϕ_1 can be determined from ρ_1 . Now ρ_1 can be used to construct $H_{\text{KS}2}$ which will yield ρ_2 , and so on. The procedure can be used until the series converge and final density ρ_f get out as shown in the flow chart in Figure (2).

Figure. (2):

Flow chart for the n^{th} iteration in the self-consistent procedure to solve Hartree-Fock or Kohn-Sham equations.



2.5 The Exchange-Correlation Functional

We do not yet know what the exchange-correlation functional is, although the Kohn-Sham diagram was an accurate description and only one approximation was made, which is the Born-Oppenheimer. Two approximations will be used to solve this unknown part. These two approximations are: LDA (Local Density Approximation) and GGA (Generalized Gradient Approximation) ^[19].

2.6 Local Density Approximation (LDA)

As mentioned earlier, the exchange-correlation function is not precisely known ^[28]. We can use the local density approximation to solve for exchange-correlation energy. The two who applied the approximate LDA to the DFT are Kohn and Sham ^[29]. The local density approximation for the exchange correlation energy can be written as the following equation:

$$E_{xc}^{LDA} = \int \rho(\vec{r}) \varepsilon_{xc}[\rho(\vec{r})] d\vec{r} \quad (13)$$

where the $\varepsilon_{xc}[\rho(\vec{r})]$ in equation (13) is defined as the exchange-correlation energy per electron of a homogenous electron gas. The electron density is precisely $\rho_0(r)$ at each point r . It is known that the LDA approximation will be valid when the electronic density varies slowly with position by the term “local” indicating that there is no $\rho_0(r)$ derivative in the expression for $\varepsilon_{xc}[\rho(\vec{r})]$ given by equation (13). If we look closely at the exchange and correlation contributions separately, then we can compute the first contribution analytically. Correlation energy, in turn, lacks analytic expression and is represented as a complex function of ρ_0 depending on the parameters whose values are fitted using a precise simulation of the homogeneous electron gas energy.

$$E_{xc}^{LDA} = E_x^{LDA} + E_c^{LDA} \quad (14)$$

The first term is the exchange energy which comes from the Pauli exclusion principle, while the second term, called the correlation energy which comes from the interaction of electrons with the same spin.

2.7 Generalized Gradient Approximation (GGA)

By including the first derivatives of the electronic density, the GGA approximation can improve the LDA definition ^[19] of the exchange-correlation energy. Regardless of the

homogeneity of the true charge density, LDA is used as the exchange energy density of a regular electron gas. By including the electron density gradient in the function, the generalized gradient is approximated taking care of such inhomogeneities. The charge density and the charge density gradient are used by this approximation to solve for the exchange-correlation energy as in equation (15).

$$E_{xc}^{GGA} = \int \rho(\vec{r}) \varepsilon_{xc}[\rho(\vec{r}), \vec{\nabla}\rho(\vec{r})] d\vec{r} \quad (15)$$

2.8 The Modified Becke-Johnson (mBJ) potential

It is a tool that is very important which is used in WIEN2k code^[30] because it improves the band structure of materials, especially semiconductor materials, and is therefore important in general agreement with the experiment. A direct optimization to obtain the lattice parameter in a consistent manner is not possible due to the lack of an exchange and correlation energy term from which to infer the mBJ-GGA potential. The deviation in the experimental gap value can reach more than 20%. To calculate the band structure and the resulting network parameter, this author suggested that the LDA, GGA optimization procedure was previously used and this option is very important because percentage differences in the lattice parameter can lead to relative deviations in the expected band gap value.

2.9 Augmented Plane Wave (APW) Method

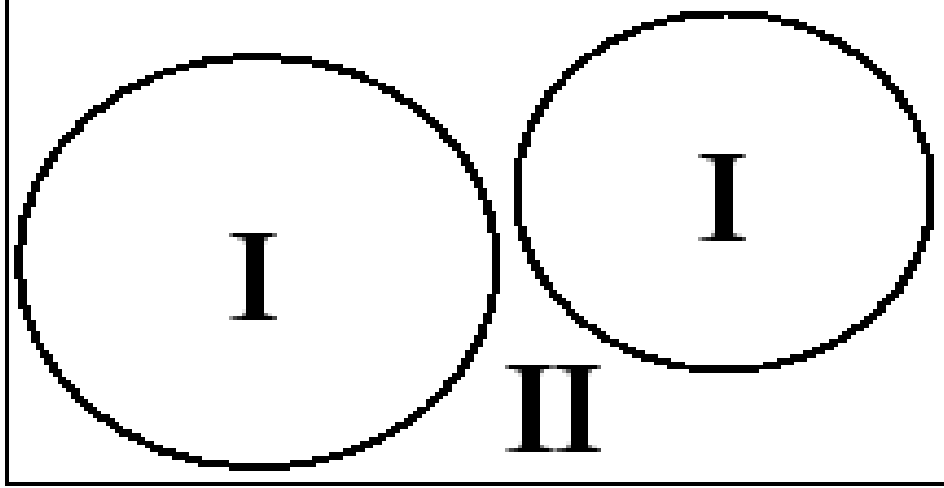
We can say that the APW method is to solve the Kohn-Sham equation^[19]. The free electrons are described by plane waves in the region far from the nuclei, while they behave just like a free atom in the region near the nucleus, therefore, it can be best described by atomic-like functions. A single cell is divided into two types of regions in the APW diagram as shown in Figure 3. i) non-overlapping spheres centered at the atomic sites such a sphere is often called a muffin tin sphere. ii) An interstitial region; the remaining space outside the spheres. APW, using the expansion of φ_n , is defined as:

$$\phi_{\vec{K}}^{\vec{k}}(\vec{r}, E) = \begin{cases} \frac{1}{\sqrt{V}} e^{i(\vec{k}+\vec{K})\cdot\vec{r}} & , \quad \text{Outside sphere} \\ \sum_{l,m} A_{lm}^{\alpha, \vec{k}+\vec{K}} u_l^{\alpha}(r', E) Y_m^l(\hat{r}') & , \quad \text{Inside sphere} \end{cases} \quad (16)$$

where \vec{k} is the wave vector inside the Brillion zone, \vec{K} is the reciprocal lattice vectors, V is the volume of the unit cell, r' is the position vector inside the sphere and finally u_l^α is the numerical solution to the radial Schrodinger equation at the energy ε .

Figure. (3)

scheme of Augmented Plane Wave.



2.10 The Linearized Augmented Plane Wave (LAPW) Method

We can also consider that the LAPW ^[19] procedure is to solve the Kohn-Sham equations for the total energy and ground state density and the Kohn-Sham eigenvalues for many electrons system by presenting a set that fits most closely with the problem. It was Anderson who proposed the LAPW diagram and he also proposed extending the energy dependence of radial wave functions $u(r')$ into atomic spheres with the energy derivative $\frac{\partial u^\alpha(r', E)}{\partial E} = \dot{u}^\alpha(r', E)$. In this scheme a linear combination of spherical harmonics for radial functions is used. The spherical harmonic is denoted by $Y_{lm}(r)$ and $u_l(r, E_l)$ is used to solve the Schrödinger equation for the radial energy E_l and the spherical part of the inner sphere of the sphere $\dot{u}^\alpha(r', E)$ is the energy derivative of u_l taken with the same energy E_l .

$$\phi_{\vec{K}}^{\vec{k}}(\vec{r}, E) = \sum_{l,m} (a_{lm}^{\alpha, \vec{k}+\vec{K}} u_l^\alpha(r', E) + b_{lm}^{\alpha, \vec{k}+\vec{K}} \dot{u}_l^\alpha(r', E)) Y_m^l(\hat{r}'), \quad \text{Inside sphere} \quad (17)$$

In the interstitial region a plane wave is used

$$\phi_{\vec{K}}^{\vec{k}}(\vec{r}, E) = \frac{1}{\sqrt{V}} e^{i(\vec{k}+\vec{K})\cdot\vec{r}}, \quad \text{Outside sphere} \quad (18)$$

We can say that, in general, the LAPW method expands the potentials as follows:

$$V(\vec{r}) = \begin{cases} \sum_{lm} V_{lm}(r) Y_{lm}(\hat{r}), & \text{inside sphere} \\ \sum_{\vec{k}} V_{\vec{k}} e^{i\vec{k} \cdot \vec{r}}, & \text{outside sphere} \end{cases} \quad (19)$$

2.11 WIEN2k code

WIEN2k code is written by two people, Blaha, Schwarz and their co-workers, the WIEN2k code is a very successful implementation of the FP-LAPW method ^[31].

Density functional theory is used to make electronic calculations for the structure of solids using WIEN2k program.

The solution of Kohn-Sham equations for density functional theory was developed by Schwarz and Blaha at the Vienna University of Technology. Generalized gradient approximation GGA or local density approximation LDA can be used in density functional theory. The above represents the relativistic effects and the diagram of all electrons.

Chapter Three

Computational method

The calculations in this work were performed using the full potential linearized augmented wave method in WIEN2k code. It was performed in two structures; one is cubic and the other is orthorhombic within a Perdew-Burke-Ernzerhof of generalized gradient approximation (PBE-GGA). In this work, we calculated the structural, electronic, magnetic and elastic properties of CeCrO₃ and CeGaO₃. Using a muffin-tin sphere of radius R_{MT} we determined the spherical harmonics around each nucleus ^[32]. And by means of lattice parameters, we determined the crystal structure of each of the mentioned compounds. Using the Murnaghan equation ^[33] of state, the following structural parameters were found: Lattice parameter, volume, Bulk modulus, first derivative of pressure and energy.

In the first structural state, which is the cubic, for the first compound CeCrO₃, the muffin-tin radii (R_{MT}) of Ce, Cr and O atoms are 2.5, 1.83 and 1.66 a.u., respectively and for the compound CeGaO₃, R_{MT} of Ce, Ga and O atoms are 2.5, 1.82 and 1.65 a.u., respectively. In the case of an orthorhombic structure, for the compound CeCrO₃, the muffin-tin radii (R_{MT}) of Ce, Cr and O atoms are 2.25, 1.9 and 1.72 a.u., respectively and for the compound CeGaO₃, R_{MT} of Ce, Ga and O atoms are 2.16, 1.78 and 1.61 a.u., respectively. The cut-off energy to separate the core states from valence states is set to be -9 Ry. Also, there are 35 special k-points in the irreducible Brillion zone with grid $10 \times 10 \times 10$ (equivalent to 1000 k-points in the Full Brillion Zone) ^[34] are used to obtain self-consistency for CeCrO₃ and CeGaO₃ compounds. Moreover, the number of plane waves was restricted by $K_{MAX} R_{MT} = 8$ and the expansions of the wave functions was set by $l=10$ inside the muffin-tin spheres.

When using the GGA approximation, the G_{max} is set to 14 with cut-off $l_{max}= 8$ and 35k points in the irreducible Brillion zone with grid $10 \times 10 \times 10$ meshes.

For the exchange-correlation potential we use PBE-GGA ^[35]. To improve the energy band gap of CeCrO₃ and CeGaO₃ the modified Becki-Johnson potential (mBJ-GGA) was used ^[36].

Chapter Four

Results and Discussion

4.1 Structural properties

To calculate the structural properties; optimized lattice constant (a), bulk modulus (B), its pressure derivative (B'), and minimum energy E_0 . The total energy (Ry) versus volume (a.u³) graphs were fitted by using Murnaghan's^[37]. Murnaghan's equation of state (EOS) is given by:

$$E(V) = E_0 + \frac{V B}{B'} \left\{ \left[\left(\frac{V_0}{V} \right)^{B'} / (B' - 1) \right] + 1 \right\} - [B V_0 / (B' - 1)] \quad (20)$$

Pressure, $P = - \frac{dE}{dV}$, Bulk modulus, $B = - V \frac{dP}{dV} = V \frac{d^2 E}{dV^2}$

Where B is the bulk modulus at the equilibrium volume, B' is the pressure derivative of the bulk modulus at the equilibrium volume and E_0 is the minimum energy.

By minimizing the total energy, we have optimized the lattice parameters of these compounds CeCrO₃ and CeGaO₃. By using the calculated optimized values of the lattice parameter constants we have calculated the structural parameters (lattice parameters, total energy bulk modulus and first pressure derivatives of bulk modulus) of these compounds in a cubic and orthorhombic perovskite structure.

We can get the structural parameters (lattice parameters, total energy bulk modulus and first pressure derivatives of bulk modulus) by plotting volume versus energy by the Murnaghan equation of state^[37] to estimate the ground state properties of these compounds.

Initially in a cubic structure, Figure 4 shows the fitted total energy versus volume for CeCrO₃ by using PBE-GGA approximation.

Figure. (4)

Equation of state of cubic perovskite of CeCrO₃ PBE-GGA methods, (E vs V)

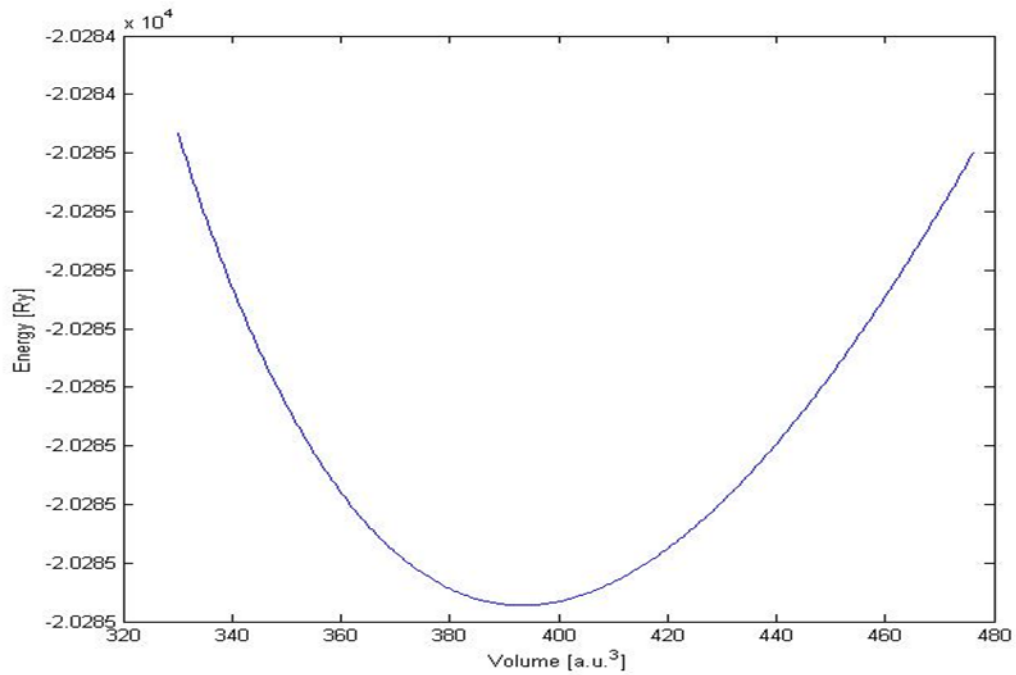


Table (1)

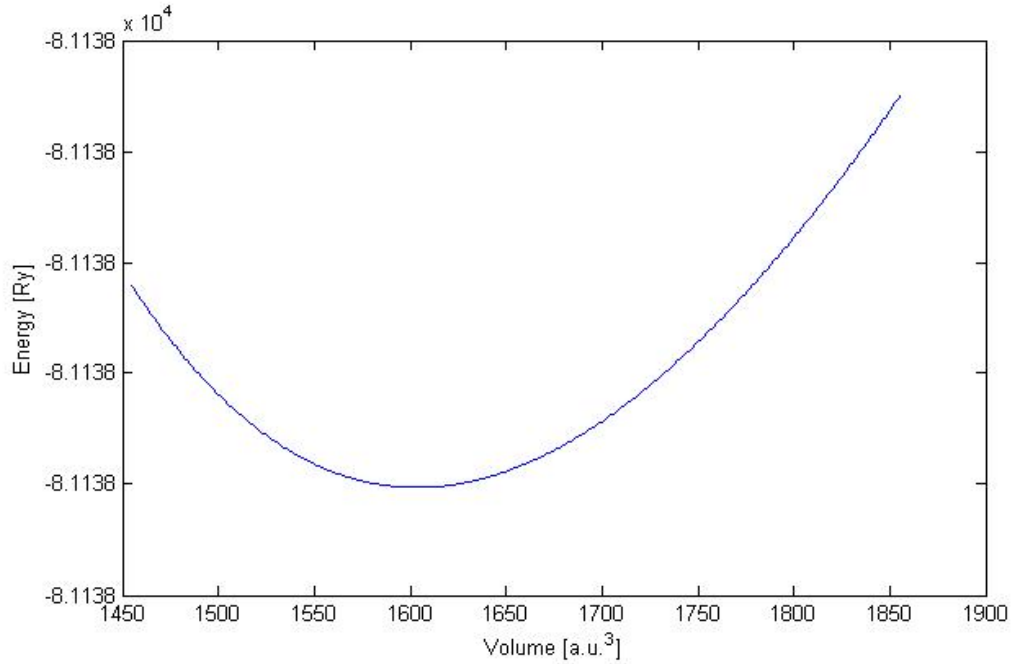
Calculated lattice parameter, bulk modulus, pressure derivative of CeCrO₃ in a cubic structure

Structure	Lattice parameter (Å ^o)		B _o (GPa)		B'
	Present	Others	Present	Others	Present
Cubic	3.8772	3.877 ^[38]	182.2342	183.81 ^[38]	4.3081

In Table 1, the present results are in good agreement with other theoretical results ^[39] for the lattice parameter and bulk modulus of cubic CeCrO₃ compound.

Figure. (5)

Equation of state of orthorhombic perovskite of CeCrO_3 PBE-GGA methods, (E vs V).

**Table (2)**

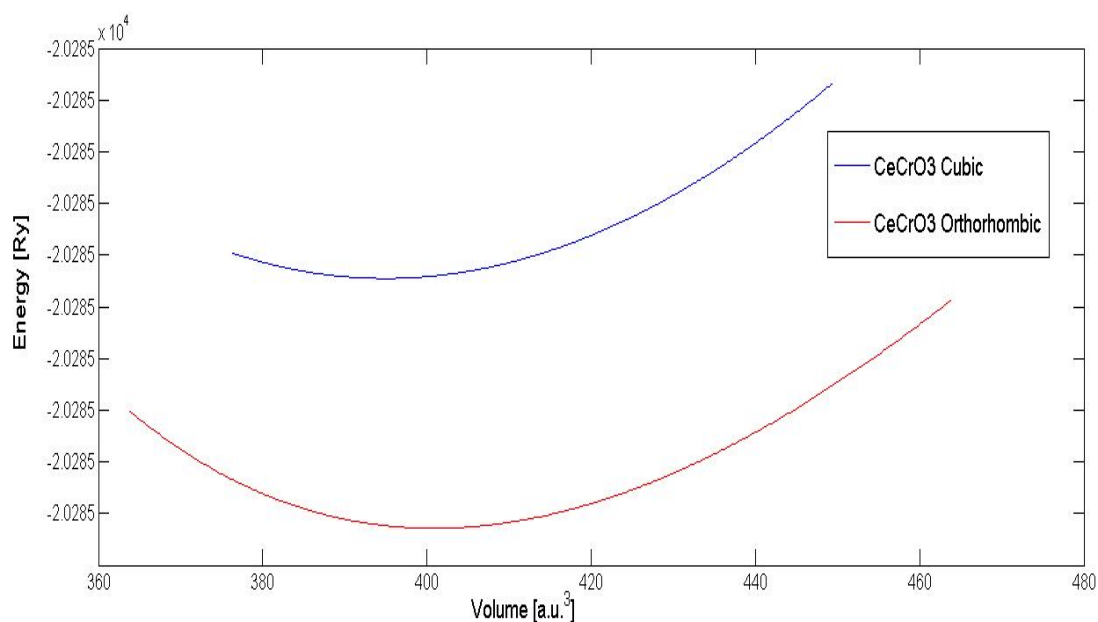
Calculated lattice parameter, bulk modulus, pressure derivative of CeCrO_3 in orthorhombic structure.

Structure	Lattice parameter(\AA°)		B_o (Gpa)		B'	
	Present	Others	Present	Others	Present	Others
Orthorhombic	a=5.6227934 b=7.6759456 c=5.3932411	a=5.897 ^[39] b=7.726 ^[39] c=5.158 ^[39]	165.5768	169.17 ^[39]	3.8973	4.86 ^[39]
Experimental Results	a=5.479 ^[40] b=7.733 ^[40] c=5.472 ^[40]		

From Table 2, the present results are in good agreement with other theoretical and experimental results, i.e., the Lattice parameter, the bulk modulus, or even for the pressure derivative. The calculated constant lattice parameter (a) of orthorhombic CeCrO_3 compound is overestimated the experimental lattice parameter with 2.5% larger^[40], while the calculated constants lattice parameter (b and c) are 0.74% and 1.46%, respectively smaller than the experimental value^[40].

Figure. (6)

The relationship between Equation of state of the Cubic and orthorhombic perovskite of CeCrO₃ PBE-GGA methods, (E vs V)



In the orthorhombic structure for CeCrO₃ using PBE-GGA approximation, this compound contains twenty atoms and the volume and energy in Figure 6 are divided by the number 4 because the compound CeCrO₃ in the case of the cubic structure contains five atoms and we did this process to see which one has less energy than the other and it shows us from figure 6 that the compound in the orthorhombic structure has lower energy. The minimum energy of the compound is -20284.61275 Ry while for the cubic structure its minimum energy is -20284.564522 Ry and this comparison is at the same muffin-tin radii (R_{MT}) of the orthorhombic structure. R_{MT} of Ce, Cr and O atoms are 2.25, 1.9 and 1.72 a.u., respectively.

In a cubic structure, Figure 6 shows the fitted total energy versus volume for CeCrO₃ by using PBE-GGA approximation.

Figure. (7)

Equation of state of cubic perovskite of CeCrO₃ PBE-GGA methods, (E vs V)

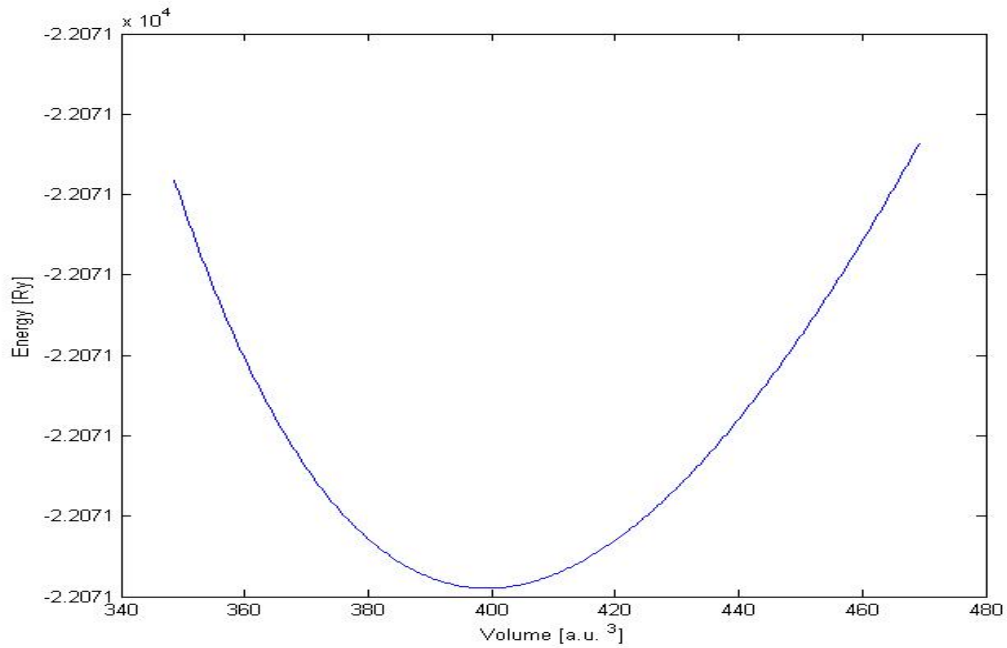


Table (3)

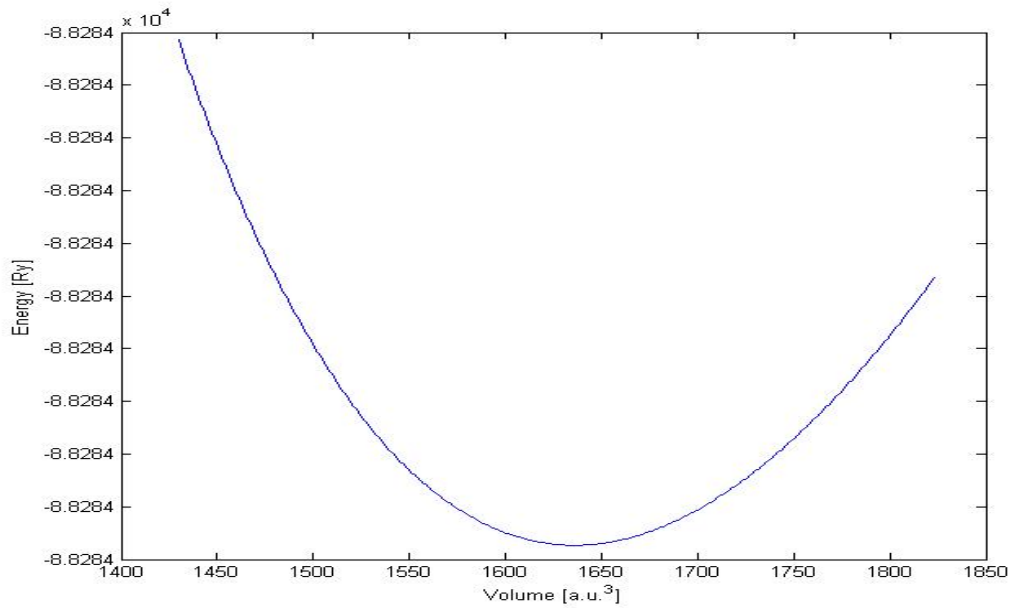
Calculated lattice parameter, bulk modulus, pressure derivative of CeGaO₃ in a cubic structure.

Structure	Lattice parameter(A°)		B ₀ (Gpa)	B'
	Present	Others	Present	Present
Cubic	3.8964	174.0224	3.0718

Table 3 shows the calculations of the lattice parameter, bulk modulus and pressure derivative of a cubic CeGaO₃ compound using PBE-GGA. The optimized lattice parameter, in particular is used to study the electronic, magnetic and elastic properties.

Figure. (8)

Equation of state of orthorhombic perovskite of CeGaO_3 PBE-GGA methods, (E vs V)

**Table (4)**

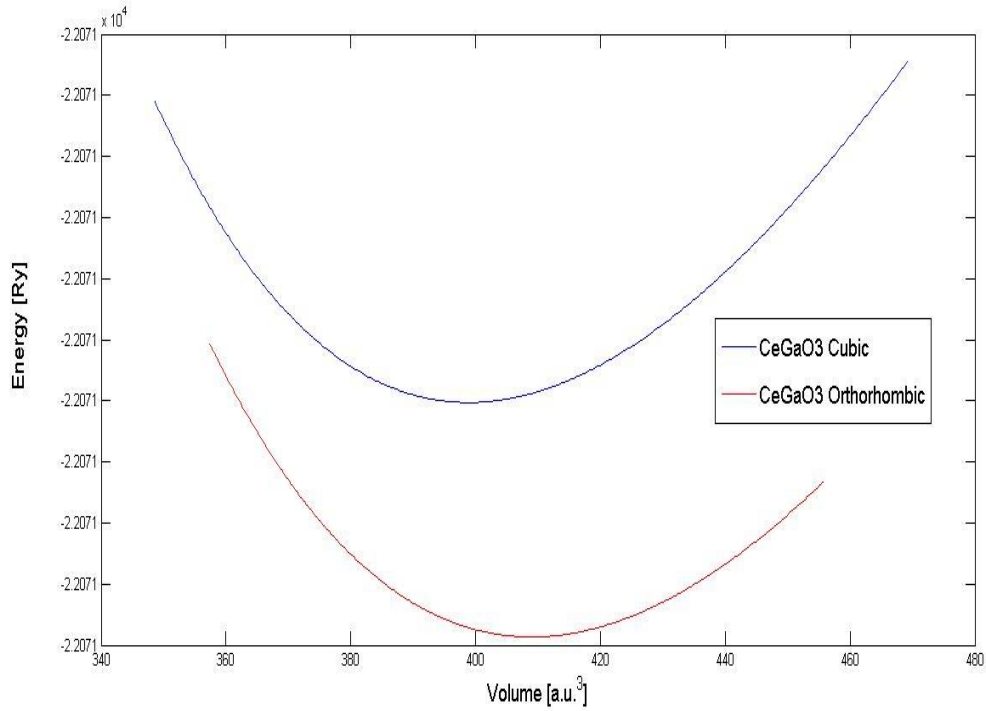
Calculated lattice parameter, bulk modulus, pressure derivative of CeGaO_3 in orthorhombic structure

Structure	Lattice parameter(\AA)		B_o (Gpa)	B'
	Present	Others	Present	Present
Orthorhombic	a=5.7510644748 b=8.1253060458 c=5.6673073582	165.5768	3.8973
Experimental Results	a=5.490 ^[41] b=7.748 ^[41] c=5.485 ^[41]		177 ^[41]

In the CeGaO_3 orthorhombic structure, the experimental results^[41] slightly overestimate the lattice parameter if we compare it with our present results and also the experimental results^[41] of the bulk modulus are slightly overestimated compared to the present results.

Figure. (9)

The relationship between Equation of state of the Cubic and orthorhombic perovskite of CeGaO₃ PBE-GGA methods, (E vs V).



In the orthorhombic structure for CeGaO₃ by using PBE-GGA approximation, we also say here, as we said about the CeCrO₃ compound, that in this structure this compound contains twenty atoms and the volume and energy in Figure 9 have been divided by the number 4 because the compound in the cubic structure case contains five atoms and we have done this process to see which one is Less energy than the other. It is shown in Figure 9 that the compound in the orthorhombic structure has less energy. The minimum energy of the compound in this case is -22071.008655 Ry while in the case of the cubic structure its minimum energy is -22070.970288 Ry and this comparison is at the same muffin-tin radii (R_{MT}). R_{MT} of Ce, Ga and O atoms are 2.16, 1.78 and 1.61 a.u., respectively.

4.2 Electronic properties

A. Band Structure

In this section, we calculate the band structure in the Brillion-zone along the high symmetry line for the two perovskite compounds CeCrO₃ and CeGaO₃ in the cubic and orthorhombic structure at zero pressure and the Fermi level is set at zero eV.

Table (5)

Energy band gap (E_g) of $CeCrO_3$ and $CeGaO_3$ compounds using PBE-GGA methods.

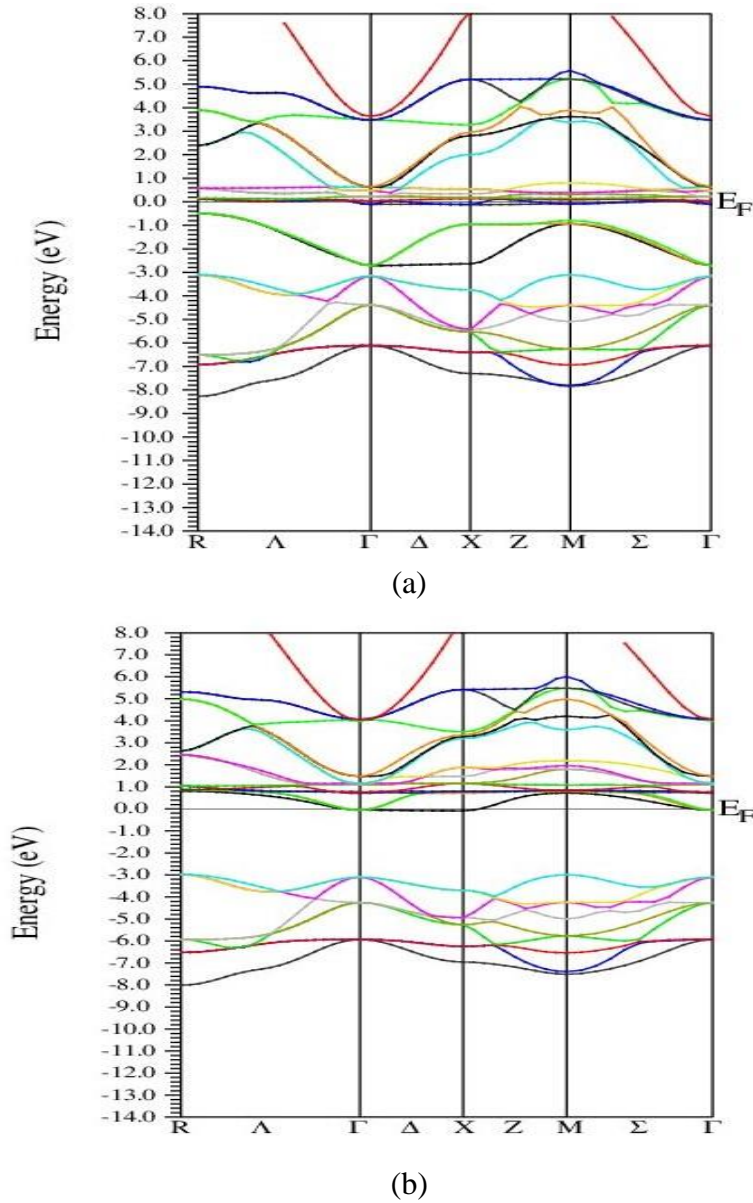
Materials	Structure	Spin	Band gapytype	Energy bandgap (eV)	Eg-mBJ	Other theoretical Results
$CeCrO_3$	Cubic	Up	Metallic	Metallic	
		Down	Indirect	M \rightarrow Γ 3	M \rightarrow X3.1	M 2.89 ^[38]
	Orthorhombic	Up	Indirect	Γ 0.9	Γ 3.013	Γ 0.9 ^[39]
		Down	Metallic	Metallic	
$CeGaO_3$	Cubic	Up	Indirect	M 0.117	M 1.261	
		Down	Indirect	M 3.144	M 3.118	
	Orthorhombic	Up	Metallic	Γ 1.346	
		Down	Indirect	Γ 3.6	Γ 4.5	

Table 5 shows us the calculation of the band gap of the cubic structure and orthorhombic of $CeCrO_3$ and $CeGaO_3$ using PBE-GGA and then we optimize the results by mBJ-GGA potential and shows us that the present results are in great agreement with the other theoretical results.

In the cubic perovskite of $CeCrO_3$ and using PBE-GGA the band structure of this compound was calculated in both spin-up and spin-down states. We found that the spin up results imply that it is metallic while in the case of spin down the valence band maximum (VBM) we find that the compound occurs along the point symmetry line M while conduction band minimum occurs along Γ -point symmetry line with energy gap 3 eV, as shown in Figure (10, a and b).

Figure. (10)

The Calculated spin polarized (a) up (b) down band structures for cubic CeCrO_3 compound using PBE-GGA.



But by using the modified Beke-Johnson potential (mBJ-GGA) we have improved the calculations of the energy band gap for this compound. In the mBJ-GGA the energy gap of CeCrO_3 compound in the case of spin-up remained metallic (as shown in Figure 11.a (see Appendix (B))) and in the case of spin-down the energy gap increased by a very small percentage to become 3.1 eV, while the compound remained semiconductor in this state, as shown in Figure (11.b) (see Appendix (B)). M. Rashid et al^[38] calculated the energy gap within the mBJ-GGA and found it to be 2.89 eV and this value is in a good agreement with our calculations.

In the orthorhombic perovskite of CeCrO_3 using PBE-GGA, the band structure for the spin up was calculated, it is found that the conduction band minimum (CBM) is 0.3 eV located at the Γ point. At the same time, the valence band maximum (VBM) is -0.6 eV at the Γ point, which gives a direct band gap energy of 0.9 eV. A. Abbad et al ^[39] used FP-LAPW method to calculate the energy gap of CeCrO_3 compound in the orthorhombic perovskite structure, and the same result appeared with them as well, which is 0.9 eV, While the energy gap is metallic in the case of spin down of this compound. So, this compound is half-metallic in PBE-GGA. In mBJ-GGA, the energy gap increased by a large percentage to become 3.013 eV in the spin-up state, while in the spin-down state the energy gap of CeCrO_3 remained metallic, so the compound in this case is also half-metallic as shown in Figure 13 (see Appendix (B)).

Figure (14) (a and b) (in Appendix (B)) shows that the band structure of the spin up and spin down of cubic perovskite of CeGaO_3 compound has an indirect energy band gap using PBE-GGA method. The indirect energy gap within PBE-GGA for the spin up and spin down is 0.117 eV and 3.144 eV respectively, so the compound in this case is a semiconductor. Also, Figure (15) (a and b) (in Appendix (B)) shows that the band structure of the spin up and the spin down of cubic CeGaO_3 compound has an indirect energy band gap using mBJ-GGA method. The indirect energy gap mBJ-GGA was found to be 1.261 eV, 3.118 eV respectively, so the compound also in this case is a semiconductor, as shown in Table 5.

Figure (16) (a and b) (in Appendix (B)) shows that the band structure of orthorhombic perovskite of CeGaO_3 compound of the spin up is metallic while the spin down has an indirect energy band gap using PBE-GGA method. The indirect energy gap within PBE-GGA for the spin down is 3.6 eV, so the compound in this case is half-metallic. Also, Figure (17) (a and b) (in Appendix (B)) shows that the band structure of the spin up and the spin down of orthorhombic CeGaO_3 compound has an indirect energy band gap using mBJ-GGA method. The indirect energy gap mBJ-GGA was found to be 1.346 eV, 4.5 eV respectively, so the compound in this case for the spin up and spin down is a semiconductor and an insulator respectively.

B. Density of state

This part of the chapter can be defined as a description of the ratio of states that the system will occupy at each energy. Also, in this part the total and partial densities of

states of CeCrO_3 and CeGaO_3 in the cubic and orthorhombic structure by using PBE-GGA were calculated.

Figure (18) (see Appendix (B)) shows a spin-up of the cubic compound CeCrO_3 using PBE-GGA, the valence band coming mainly from Cr-d and with little contribution of O-p, while the conduction band originates from Ce-f and little Cr-d. And Figure (19) (see Appendix (B)), in the spin-down state, the valence band comes from O-p and with a little contribution from Cr-d, while the conduction band originates from Ce-f and Cr-d.

Figure (20) (in Appendix (B)) shows a spin-up of the cubic compound CeCrO_3 with mBJ-GGA potential, the valence band coming mainly from Cr-d and with small contribution of O-p, while the conduction band originates from Ce-f and little Cr-d. Figure (21) (see Appendix (B)), in the spin-down state the valence band comes from O-p and with a little contribution from Cr-d, while the conduction band originates from Ce-f and Cr-d.

Figure (22) (in Appendix (B)) shows a spin-up of the orthorhombic compound CeCrO_3 using PBE-GGA, the valence band coming mainly from Cr-d and with little contribution of O-p, while the conduction band originates from Ce-f and little Cr-d. Figure (23) (in Appendix (B)) shows that in the spin-down state the valence band comes from O-p and with a little contribution from Cr-d, while the conduction band originates from Ce-f and Cr-d.

Figure (24) (in Appendix (B)) shows a spin-up of the orthorhombic compound CeCrO_3 with mBJ-GGA potential, the valence band coming mainly from Cr-d and with small contribution of O-p, while, the conduction band originates from Ce-f and little Cr-d. And in Figure (25) -(in Appendix (B)), the spin-down state shows that the valence band comes from O-p and with a little contribution from Cr-d, while the conduction band originates from Ce-f and Cr-d.

Figure (26) (in Appendix (B)) shows a spin-up of the cubic compound CeGaO_3 using PBE-GGA, the valence band coming mainly from Ga-d and with little contribution of Ce-p and O-p, while the conduction band originates from Ce-f and little O-p. And Figure (27) (in Appendix (B)), in the spin-down state the valence band comes from O-p and Ga-d, while the conduction band originates from Ce-f and with small contribution of O-p.

Figure (28) (in Appendix (B)) shows a spin-up of the cubic compound CeGaO_3 with mBJ-GGA potential, the valence band coming mainly from Ga-d and with small contribution of Ce-p and O-p, while the conduction band originates from Ce-f and little O-p and Ce-d. Figure (29) (in Appendix (B)) , in the spin-down state the valence band comes from O-p and Ga-d with small contribution of Ce-p, while the conduction band originates from Ce-f with small contribution of O-p and Ce-d.

Figure (30) (in Appendix (B)) shows a spin-up of the orthorhombic compound CeGaO_3 using PBE-GGA, the valence band coming mainly from Ga-s, Ga-p and Ga-d and with little contribution of O-p, while the conduction band originates from Ce-f and little Ga-s and Ga-p. Figure (31) (see Appendix (B)) in the spin-down state the valence band comes from O-p and with a little contribution from Ga-s, Ga-p and Ga-d, while the conduction band originates from Ce-f and Ga-p and to a lesser extent in Ga-s.

Figure (32) (in Appendix (B)) shows a spin-up of the orthorhombic compound CeGaO_3 with mBJ-GGA potential, the valence band coming mainly from Ga-d and with small contribution of Ce-p and O-p. While the conduction band originates from Ce-f and little Ce-d. And in Figure (33) (see Appendix (B)), the spin-down state the valence band comes from Ga-d and with a little contribution from Ce-p and O-p, while the conduction band originates from Ce-f and with small contribution of Ce-d and O-p.

4.3 Magnetic Properties

In this section, we calculated the total and partial magnetic moments of the cubic and orthorhombic CeCrO_3 and CeGaO_3 compounds and compared them with other theoretical results as shown in Tables 6 and 7 and it can be said from these results that these two compounds are ferromagnetic compounds. From these tables it is clear that our results agree very well with other theoretical results.

Table (6)

The total magnetic moment for Cubic and Orthorhombic CeCrO_3 compound using PBE-GGA method.

Compounds		Magnetic Moment (μ_B)					Total magnetic moment (M^{tot}) μ_B
		Ce	Cr	O	O	Interstitial	
Cubic CeCrO_3	Present	1.05679	2.33102	0.02807	--	0.49577	3.96778
Orthorhombic CeCrO_3	Present	-0.59622	2.20447	0.04245	0.04110	1.06095	7.99255
	Theoretical Result	-0.65 ⁽³⁹⁾	2.25 ⁽³⁹⁾	0.038 ⁽³⁹⁾	0.028 ⁽³⁹⁾	1.22 ⁽³⁹⁾	8 ⁽³⁹⁾

Table (7)

The total magnetic moment for Cubic and Orthorhombic CeCrO_3 compounds with mBJ-GGA potential.

Compounds		Magnetic Moment (μ_B)					Total magnetic moment (M^{tot}) μ_B
		Ce	Cr	O	O	Interstitial	
Cubic CeCrO_3	Present	0.98083	2.47995	0.07067	--	0.32724	4.00004
	Theoretical Result	0.9831 ⁽³⁸⁾	2.5283 ⁽³⁸⁾	0.0642 ⁽³⁸⁾	--	--	4.0004 ⁽³⁸⁾
Orthorhombic CeCrO_3	Present	-0.89228	2.52829	0.04856	0.04712	0.88502	8.00025

Tables 8 and 9 show that the total and partial magnetic moment for cubic and orthorhombic CeGaO_3 compounds were calculated by using both PBE-GGA and mBJ-GGA potentials. We found that the total magnetic moment values for CeGaO_3 ranged from 1 to 4 μ_B , which means that the compound is ferromagnetic in both cubic and orthorhombic states.

Table (8)

The total magnetic moment for Cubic and Orthorhombic CeGaO₃ compounds by using PBE-GGA method.

Compounds		Magnetic Moment (μ_B)					Total magnetic moment (M^{tot}) μ_B
		Ce	Ga	O	O	Interstitial	
Cubic CeGaO ₃	Present	0.98327	0.00116	-0.00799	--	0.04083	1.00128
Orthorhombic CeGaO ₃	Present	0.94338	0.00096	-0.00575	-0.00732	0.30220	3.99799

Table (9)

The total magnetic moment for Cubic and Orthorhombic CeGaO₃ compounds with mBJ-GGA potential.

Compounds		Magnetic Moment (μ_B)					Total magnetic moment (M^{tot}) μ_B
		Ce	Ga	O	O	Interstitial	
Cubic CeGaO ₃	Present	0.95565	-0.00009	0.01127	--	0.01066	1.00001
Orthorhombic CeGaO ₃	Present	0.94104	-0.00008	0.00723	0.00693	0.15188	4.00003

4.4 Elastic properties

In this section, we have calculated the elastic properties of CeCrO₃ and CeGaO₃ in the cubic and orthorhombic crystal. These properties are volume modulus (B), shear modulus (S), elastic constants (C_B), B/S ratio, Poisson's ratio, Young's modulus (Y) and anisotropic factor (A). The standard mechanical stability for cubic crystal is^[42]

$$C_{11} > 0, C_{11} + 2C_{12} > 0, C_{11} - C_{12} > 0 \text{ and } C_{44} > 0 \quad (21)$$

Where C_{11} is the modulus for axial compression, C_{12} is the modulus for dilation on compression and C_{44} is the shear modulus.

In this section we have calculated the elastic properties under zero pressure. From our calculations in Table (10) for the two compounds CeCrO₃ and CeGaO₃ for the case of cubic, it appears that the two compounds are stable.

To calculate the volume modulus and shear modulus, we have used the Voigt approximation^[43] and from the following equation we can calculate the Voigt shear modulus S_v :

$$S_v = \frac{1}{5}(C_{11} - C_{12} + 3C_{44}) \quad (22)$$

And for the cubic structure, the Bulk modulus is given by:

$$B = \frac{1}{3}(C_{11} + 2C_{12}) \quad (23)$$

Young's modulus (Y) can be defined as the ratio of stress to strain and is given by the following equations:

$$Y = \frac{9BS_v}{(S_v + 3B)} \quad (24)$$

Poisson's ratio and Anisotropic factor are defined by the following equations:

$$\nu = \frac{3B - 2S_v}{2(3B + S_v)} \quad (25)$$

$$A = \frac{2C_{44}}{C_{11} - C_{12}} \quad (26)$$

The hardness of materials is measured by the shear modulus and the bulk modulus^[44]. The nature of the material if it is ductile or brittle can be determined from the ratio B/S. The material with a B/S ratio greater than 1.75 is a material that behaves in a ductile nature, but if it is otherwise, the material behaves with a brittle nature^[45]. From our calculations in Table (10), the B/S ratio of the two compounds CeCrO₃ and CeGaO₃ was 2.459, 2.421, respectively, so the two compounds in this case behave in a ductile nature.

We use Poisson's ratio to get a good idea of the nature of bonding forces and from another perspective to see how stable the material is. We can determine if the bonds in compounds are ionic or covalent by calculating the value of the Poisson's ratio of the compound. If its value is greater than 0.25, the compound contains ionic bonds, while if the value of Poisson's ratio is less than that, the bonds of the compound are covalent. We have a Poisson's ratio value for the two compounds CeCrO₃ and CeGaO₃ which is 0.321 and 0.318 respectively, so the two compounds in this case have ionic bonds.

To measure the degree of anisotropy of materials an important factor is the elastic anisotropy^[46]. When the value of A is unity, the material is considered isotropic, but if its value is otherwise, the material is considered to have an elastic anisotropy^[47]. From the current results that appear in Table (10), the compound CeCrO₃ which has a value of 0.194 is anisotropic, while the compound CeGaO₃ which has a value of 0.999 is isotropic.

Table (10)

Calculated elastic constants of CeCrO₃ and CeGaO₃ in the cubic structure.

Materials	C ₁₁ (GPa)	C ₁₂ (GPa)	C ₄₄ (GPa)	B (GPa)	S (GPa)	B/S	Y (GPa)	<i>v</i>	A
CeCrO ₃	357.893	82.968	26.680	174.609	70.993	2.459	187.559	0.321	0.194
CeGaO ₃	258.5404	120.8277	68.8503	166.732	68.85272	2.421	181.565	0.318	0.999

The standard mechanical stability for orthorhombic crystal is^{[48][49]}

$$(C_{11} + C_{22} - 2C_{12}) > 0, (C_{11} + C_{33} - 2C_{13}) > 0, (C_{22} + C_{33} - 2C_{23}) > 0, C_{11} > 0, C_{22} > 0, C_{33} > 0, C_{44} > 0, C_{55} > 0, C_{66} > 0, (C_{11} + C_{22} + C_{33} + 2C_{12} + 2C_{13} + 2C_{23}) > 0 \quad (27)$$

Table (11) (in Appendix (A)) show the elastic constants for CeCrO₃ and CeGaO₃ in orthorhombic structure and from these results we found the two compounds are mechanically unstable.

Chapter 5

Conclusions

We studied the structural, electronic, magnetic and elastic properties of the two CeCrO_3 and CeGaO_3 compounds in both cubic and orthorhombic structures using PBE-GGA method. We demonstrated from the results and drawings that the two compounds are in an orthorhombic structure of less energy than in a cubic structure.

In the electronic properties, CeCrO_3 was half-metallic in its cubic structure in the PBE-GGA method. It is also half-metallic by using mBJ-GGA potential. In an orthorhombic structure the compound appeared to be half-metallic using mBJ-GGA potential, which means that the compound is of half-metallic nature.

CeGaO_3 in cubic structure is of semiconducting nature in PBE-GGA and we confirmed that by mBJ-GGA potential. While, in an orthorhombic structure it is half-metallic when using the PBE-GGA method, but when using mBJ-GGA potential it is found to be a semiconductor in its spin-up state and an insulator in spin-down state.

Magnetic properties show that the two compounds in all cases are ferromagnetic. The CeCrO_3 compound in the cubic and orthorhombic structures using the PBE-GGA method have a total magnetic moment of $3.96778 \mu_B$ and $7.99255 \mu_B$, respectively. In the case of mBJ-GGA potential, the total magnetic moment of the cubic and orthorhombic structures is $4 \mu_B$ and $8.00025 \mu_B$, respectively. Whereas, the compound CeGaO_3 in the cubic and orthorhombic structures using PBE-GGA method have a total magnetic moment of $1.00128 \mu_B$ and $3.99799 \mu_B$, respectively. In the case of mBJ-GGA potential, the total magnetic moment of the cubic and orthorhombic structures for this compound is $1 \mu_B$ and $4 \mu_B$, respectively.

In addition, we studied the elastic properties of both compounds in the cubic and orthorhombic structure. In the cubic structure, the two compounds were mechanically stable, and from the ratio B/S, we found that the two compounds have a ductile nature. It was also shown by Poisson's ratio values that the two compounds have ionic bonds. But anisotropic factor shows that the compound CeCrO_3 is elastic anisotropic and the compound CeGaO_3 is isotropic. In the orthorhombic structure, the two compounds are found to be mechanically unstable.

References

- [1] Cheng, Z., Lin, J., 2010. Layered organic–inorganic hybrid perovskites: structure, optical properties, film preparation, patterning and templating engineering. *Cryst. Eng. Commun.* 12, 2646–2662.
- [2] Wenk, Hans-Rudolf, Bulakh, Andrei, 2004. *Minerals: Their Constitution and Origin*. Cambridge University Press, New York, NY, p. 413.
- [3] Szuromi, P., and Grocholski, B., 2017. Natural and engineered perovskites. *Science* 358 (6364), 732–733.
- [4] Atta, N.F., Galal, Ahmed, El-Ads, Ekram H., 2016. Perovskite nanomaterials – synthesis, characterization, and applications. *Tech. Chapter 4*, 108–151.
- [5] Tsunoda, Y., Sugimoto, W., Sugahara, Y., 2003. Intercalation behavior of nalkylamines into a protonated form of a layered perovskite derived from aurivillius phase $\text{Bi}_2\text{SrTa}_2\text{O}_9$. *Chem. Mater.* 15, 632–635.
- [6] Zhu, J., Li, H., Zhong, L., Xiao, P., Xu, X., Yang, X., Zhao, Z., Li, J., 2014. Perovskite oxides: preparation, characterizations, and applications in heterogeneous catalysis. *ACS Catal.* 4, 2917–2940.
- [7] Nagata, S., Katsui, H., Hoshi, K., Tsuchiya, B., Toh, K., Zhao, M., Shikama, T., Hodgson, E., 2013. Recent research activities on functional ceramics for insulator, breeder and optical sensing systems in fusion reactors. *J. Nucl. Mater.* 442, S501–S507.
- [8] Kreisel, J., Glazer, A., Jones, G., Thomas, P., Abello, L., Lucazeau, G., 2000. An X-ray diffraction and Raman spectroscopy investigation of A-site substituted perovskites compounds: the $(\text{Na}_{1-x}\text{K}_x)_{0.5}\text{Bi}_{0.5}\text{TiO}_3$ ($0 < x < 1$) solid solution. *J. Phys.: Condens. Matter* 12, 3267.
- [9] Xu, B., Yin, K., Lin, J., Xia, Y., Wan, X., Yin, J., Bai, X., Du, J., Liu, Z., 2009. Room temperature ferromagnetism and ferroelectricity in Fe-doped BaTiO_3 . *Phys. Rev. B* 79.
- [10] Nenasheva, E., Kanareykin, A., Kartenko, N., Dedyk, A., Karmanenko, S., 2004. Ceramics materials based on (Ba, Sr) TiO_3 solid solutions for tunable microwave devices. *J. Electroceram.* 13, 235–238.

- [11] Protesescu, L., Yakunin, S., Bodnarchuk, M.I., Krieg, F., Caputo, R., Hendon, C.H., Yang, R.X., Walsh, A., Kovalenko, M.V., 2015. Nanocrystals of cesium lead halide perovskites (CsPbX_3 , X= Cl, Br, and I): novel optoelectronic materials showing bright emission with wide color gamut. *Nano Lett.* 15, 3692–3696.
- [12] Pengfei, Fu, Shan, Qingsong, Shang, Yuequn, Song, Jizhong, Zeng, Haibo, Ning, Zhijun, Gong, Jinkang, 2017. Perovskite nanocrystals: synthesis, properties and applications. *Sci. Bull.* 62, 369–380.
- [13] Atta, N.F., Galal, Ahmed, El-Ads, Ekram H., 2016. Perovskite nanomaterials – synthesis, characterization, and applications. *Tech. Chapter 4*, 108–151.
- [14] Khajonrit, Jessada, Wongpratad, Unchista, Kidkhunthod, Pinit, Pinitsoontorn, Supree, Maensiri, Santi, 2018. Effects of Co doping on magnetic and electrochemical properties of BiFeO_3 nanoparticles. *J. Magnetism Mag. Mater.* 449, 423–434.
- [15] Tan, K.W., Moore, D.T., Saliba, M., Sai, H., Estroff, L.A., Hanrath, T., Snaith, H.J., Wiesner, U., 2014. Thermally induced structural evolution and performance of mesoporous block copolymer-directed alumina PSCs. *ACS Nano* 8, 4730–4739.
- [16] Zuo, Chuantian, Ding, Liming, 2017. Lead-free perovskite materials $(\text{NH}_4)_3\text{Sb}_2\text{I}_x\text{Br}_{9-x}$. *Angew. Chem. Int. Ed.* 56, 6528–6532.
- [17] Shi, Zhengqi, Jayatissa, Ahalapitiya H., 2018. Perovskites-based solar cells: a review of recent progress, materials and processing methods. *Materials* 11 (5), 729–743.
- [18] Ono, Luis K., Juarez-Perez, Emilio J., Qi, Yabing, 2017. Progress on perovskite materials and solar cells with mixed cations and halide anions. *ACS Appl. Mater. Interfaces* 9, 30197–30246.
- [19] Blaha P., Schwarz K., Georg K., Madsen H., Kvasnicka D., Luitz J., Laskowski R., Tran F. and Laurence D., 2019. An Augmented PlaneWave Plus Local Orbitals Program for Calculating Crystal Properties, User's Guide, WIEN2k 19.1.
- [20] Schwarz K., 2003. DFT calculations of solids with LAPW and WIEN2k, Institute of Materials Chemistry, Vienna University of Technology.
- [21] Born, M. & Oppenheimer, J. R. Zurquantentheorie der molekeln, 1927. *Ann. Phys.* 84, 457–484.

- [22] Ziman, J. M., 1960. *Electrons and Phonons* (Oxford Univ. Press, Oxford).
- [23] Pisna, M. Lazzeri, C.Casiraghi , K.Novesolve , A. Giem ,C. Andrea, 2007. “Breakdown of the adiabatic Born–Oppenheimer approximation in grapheme”. *Nature Materials* 6, 198–201.
- [24] Coulson, 1960. *Review Modern Physics*. 48, 553.
- [25] Koch, MC. Holthausen, 2000. *A chemist’s guide to density functional theory*. Wiley-VCH, Weinheim.
- [26] Parr, W. Yang, *Density functional theory of atoms and molecules*. Oxford University Press, Oxford 1989.
- [27] Orio, D. Pantazis, F.Neese, 2009.” *Density functional theory” Photosynthesis research*. 102:443-453.
- [28] Hohenberg, W.Kohn, 1964. *Physical. Review*.136,864-871.
- [29] Kohn and L. J. Sham, 1965. *Physical. Review* .140, A1113.
- [30] Camargo-Martinez J. A. and Baquero R. 2012, Performance of the modified Becke-Johnson potential, *Materials Science*.
- [31] Blaha, K. Schwarz, P. Sorantin, S.B. Trickey, 1990. *Comput. phys. commun*,59 .399.
- [32] Tariq, A. Ahmad, S. Saad, S. Tariq, 2015.” *Structural, electronic and elastic properties of the cubic CaTiO₃ under pressure: A DFT study”*,*American Institute of Physics* 5(7).
- [33] Murnghan. *Proc. Natl. Acad. Sci*. 1944. USA 30(244).
- [34] Blaha P., Schwarz K., Madsen G., Kvasnika D. and Luitz J., 2001. *WIEN2k*, Technical Universitat Wien, Austria, ISBN 3-9501031-1-2.
- [35] Perdew, K. Burke and M, Ernzerhof, 1996. *Phys. Rev. Lett*.Vol. 77,3865.
- [36] Becke and E. R. Johnson, *J. Chem.*, 2006. *Phys*. 124, 221101.
- [37] Murnaghan F.D., 1944 *The compressibility of media under extreme pressures*.*Proc. Natl. Acad. Sci. U.S.A.*, 30, p. 244.

- [38] Rashid, M.A. Iqbal, N. A. Noor, 2017. “DFT-mBJ study of electronic and magnetic properties of cubic CeCrO₃ compound: an ab-initio investigation” Phys. Rev. Vol. 1 (1) 2017 22- 26.
- [39] Abbad, A.; Benstaali, W.; Bentounes, H.A.; Bentata, S.; Benmalem, Y., 2016. Search for half-metallic ferromagnetism in orthorhombic Ce (Fe/Cr) O₃ perovskites. Solid State Commun, 228, 36–42. doi: 10.1016/j.ssc.2015.12.005.
- [40] Shukla, R., Bera, A. K., Yusuf, S. M., Deshpande, S. K., Tyagi, A. K., Hermes, W., Pöttgen, R., 2009. Multifunctional Nanocrystalline CeCrO₃: Antiferromagnetic, Relaxor, and Optical Properties. The Journal of Physical Chemistry C, 113(29), 12663–12668.
- [41] Dahani, A., Alamri, H., Merabet, B., Zaoui, A., Kacimi, S., Boukourt, A., & Bejar, M., 2017. Electronic structure and magnetic properties of rare-earth perovskite gallates from first principles. Chinese Physics B, 26(1), 017101.
- [42] Galanakis, I. 2002. Surface properties of the half-and full-Heusler alloys. Journal of Physics: Condensed Matter, 14(25), 6329–6340. doi:10.1088/0953-8984/14/25/303.
- [43] Voigt W., Kristallphysik L. and Teubner B.G., 1850.Berlin, Germany, 1910, p.
- [44] D. Teter.,2013.” Computational alchemy: the search of new superhardmaterial “MRS Bulliten Cambridge university Press 23(1):22-27.
- [45] Pettifor, Mater. Sci. Technol. 1992. 8, 345–349.
- [46] Zener C., 1948. Elasticity and Anelasticity of Metals, University of Chicago Press, Chicago.
- [47] Ravindran P., Fast L., Korzhavyi P.A. and Johansson B., 1998. Density functional theory for calculation of elastic properties of orthorhombic crystals: application to TiSi₂, J. Appl. Phys. 84 ,4891.
- [48] Gerward, J.S. Olsen, L. Petit, G. Vaitheeswaran, V. Kanchana, A. Svane, J. Alloy, 2005. Compd. 400 56-61.
- [49] Gurel, R. Eryigit, 2006. Phys. Rev. B, 74, 014302.

Appendices

Appendice (A)

Tables

Table (11)

Calculated elastic constants of CeCrO₃ and CeGaO₃ in the orthorhombic structure.

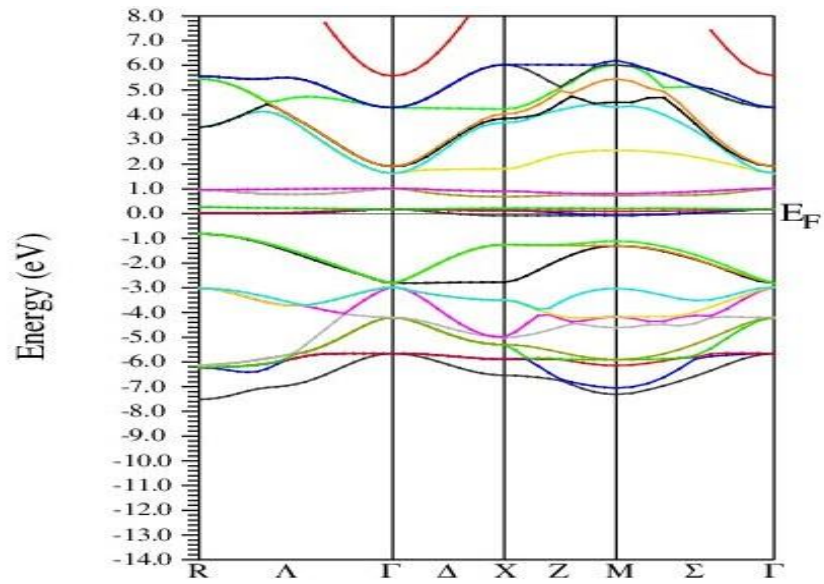
Materials	C_{11} (GPa)	C_{22} (GPa)	C_{33} (GPa)	C_{44} (GPa)	C_{55} (GPa)	C_{66} (GPa)	C_{12} (GPa)	C_{13} (GPa)	C_{23} (GPa)
CeCrO ₃	34.5	-5.9	-218.1	19.4	86.6	71.3	-77.8	-118.6	-250.7
CeGaO ₃	169.5	12.3	-1105.7	-97.3	96.9	126.6	-13.3	-39.4	-25.7

Appendice (B)

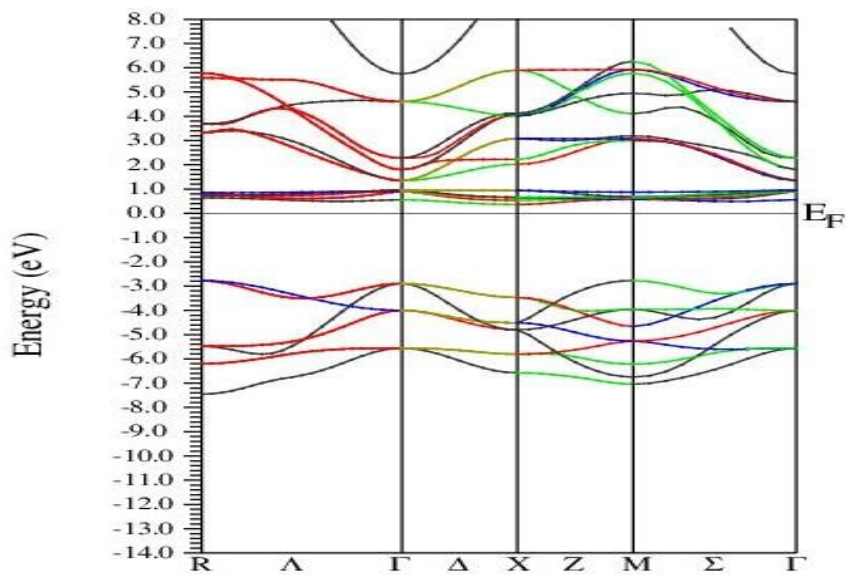
Figures

Figure. (11)

The Calculated spin polarized (a) up (b) down band structures for cubic CeCrO₃ compound with mBJ-GGA potential.



(a)



(b)

Figure. (12)

The Calculated spin polarized (a) up (b) down band structures for orthorhombic CeCrO_3 compound using PBE-GGA.

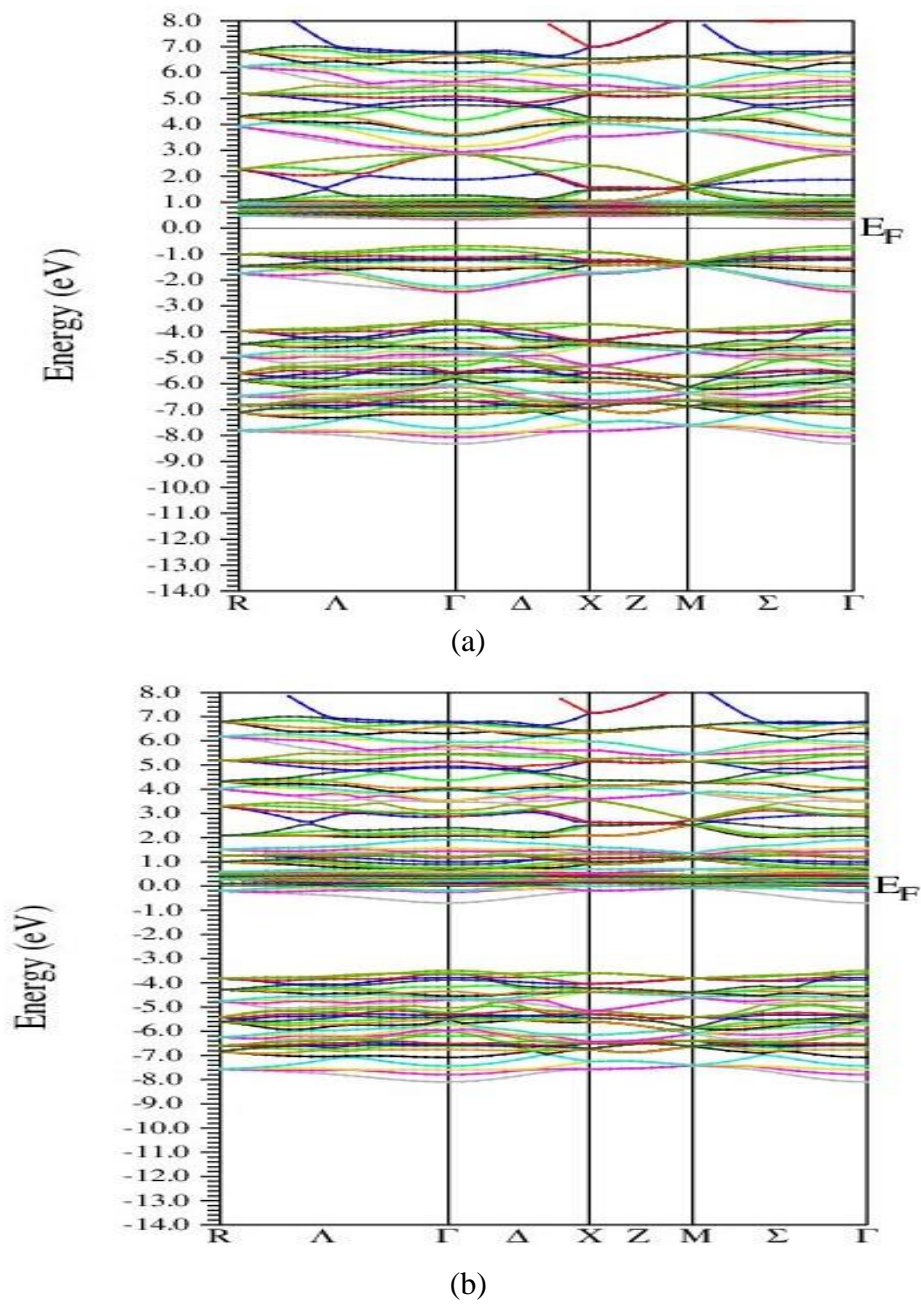
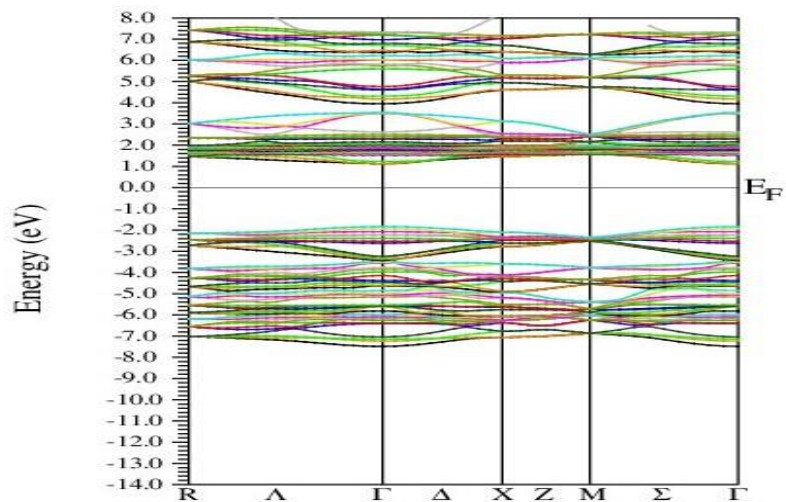
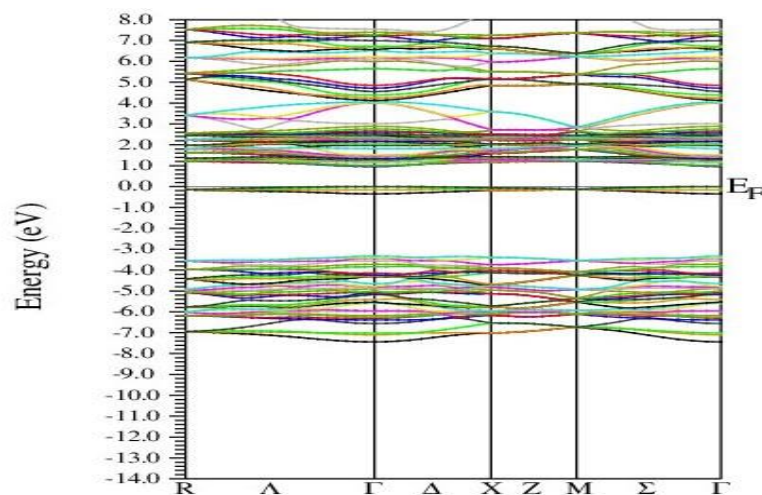


Figure. (13)

The Calculated spin polarized (a) up (b) down band structures for orthorhombic CeCrO_3 compound with mBJ-GGA potential.



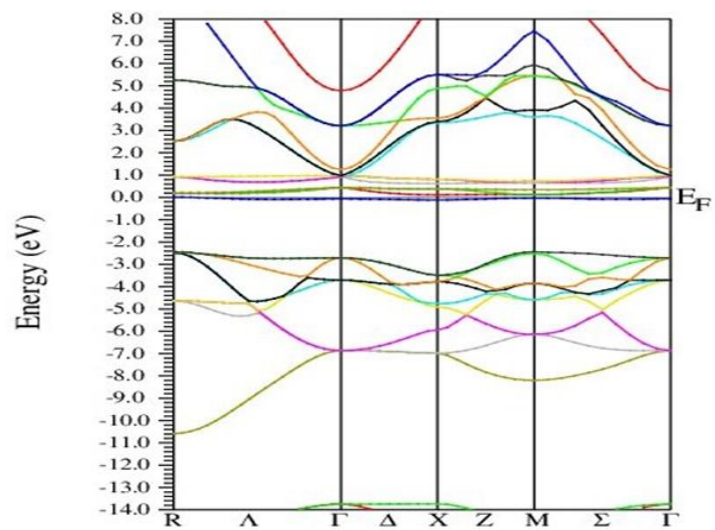
(a)



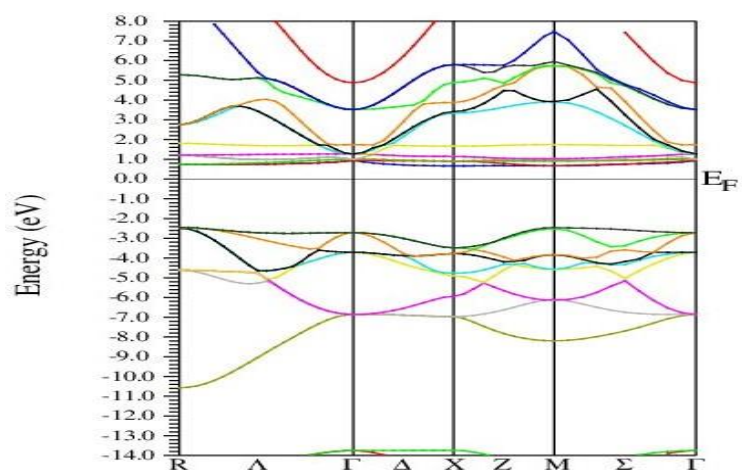
(b)

Figure. (14)

The Calculated spin polarized (a) up (b) down band structures for cubic $CeGaO_3$ compound using PBE-GGA.



(a)



(b)

Figure. (15)

The Calculated spin polarized (a) up (b) down band structures for cubic CeGaO_3 compound with mBJ-GGA potential.

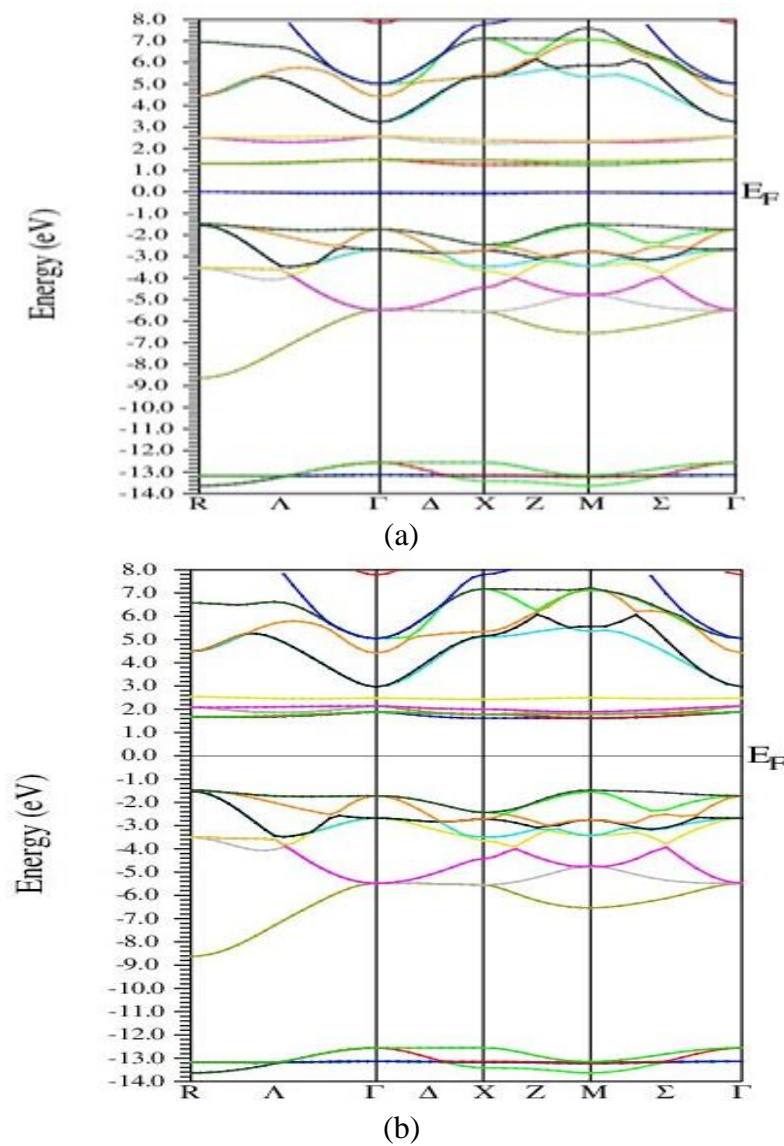


Figure. (16)

The Calculated spin polarized (a) up (b) down band structures for orthorhombic CeGaO_3 compound using PBE-GGA.

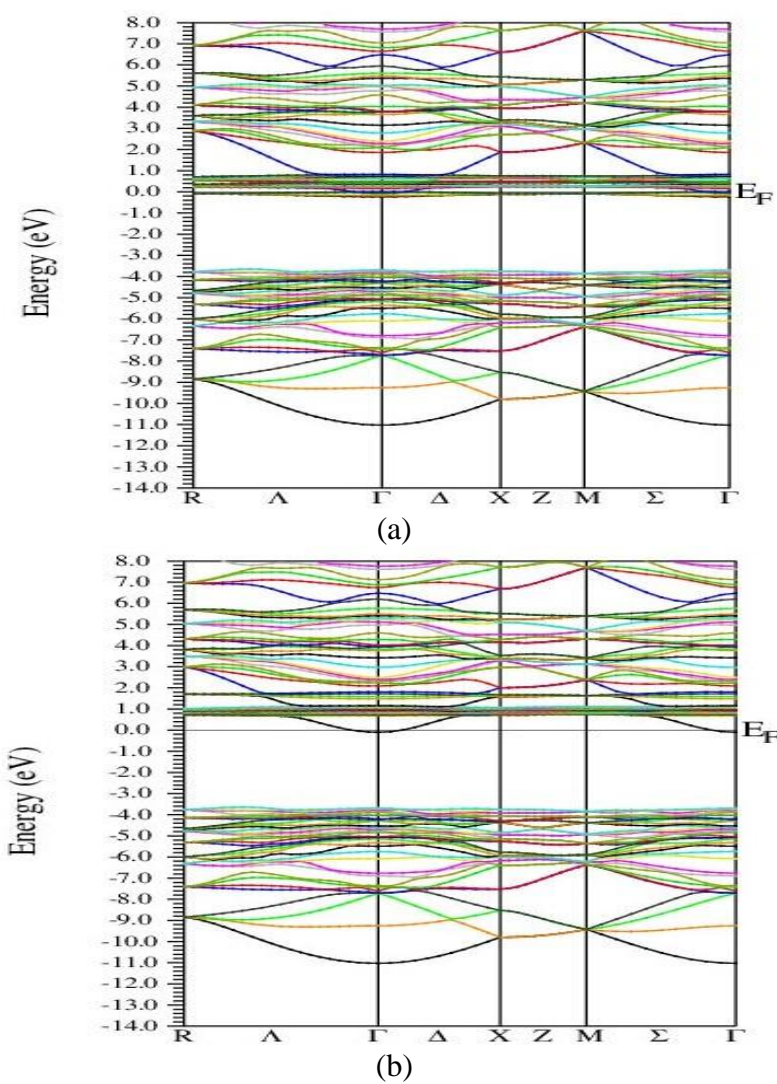


Figure. (17)

The Calculated spin polarized (a) up (b) down band structures for orthorhombic $CeGaO_3$ compound with mBJ-GGA potential.

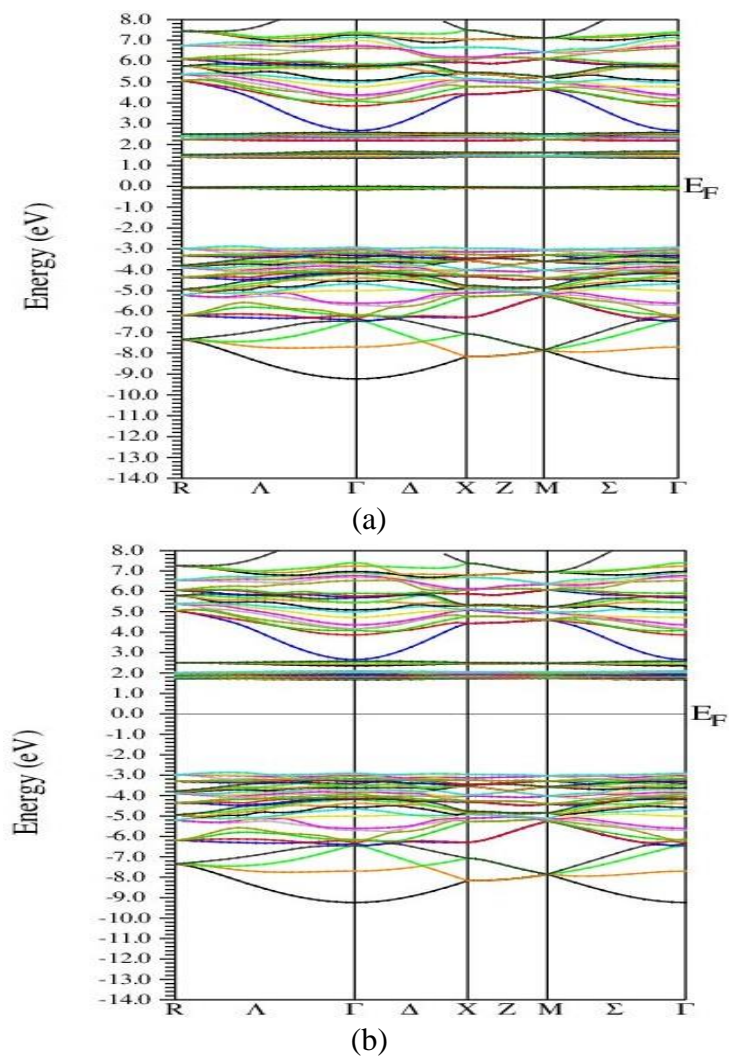


Figure. (18)

Total and partial density of state of spin up for (a) CeCrO_3 , (b) Ce, (c) Cr and (d) O of cubic CeCrO_3 compound by using PBE-GGA method.

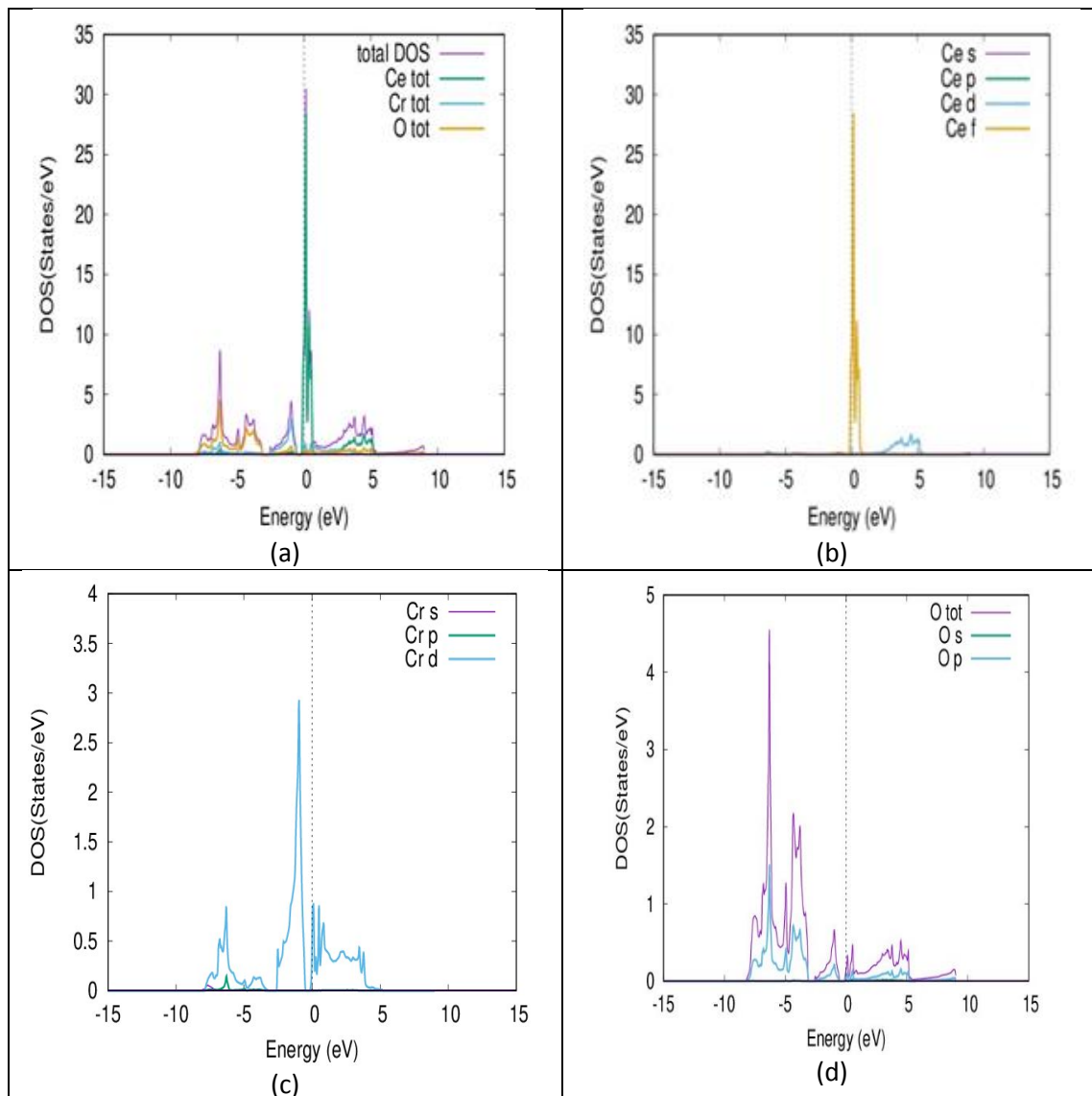


Figure. (19)

Total and partial density of state of spin down for (a) CeCrO_3 , (b) Ce, (c) Cr and (d) O of cubic CeCrO_3 compound by using PBE-GGA method.

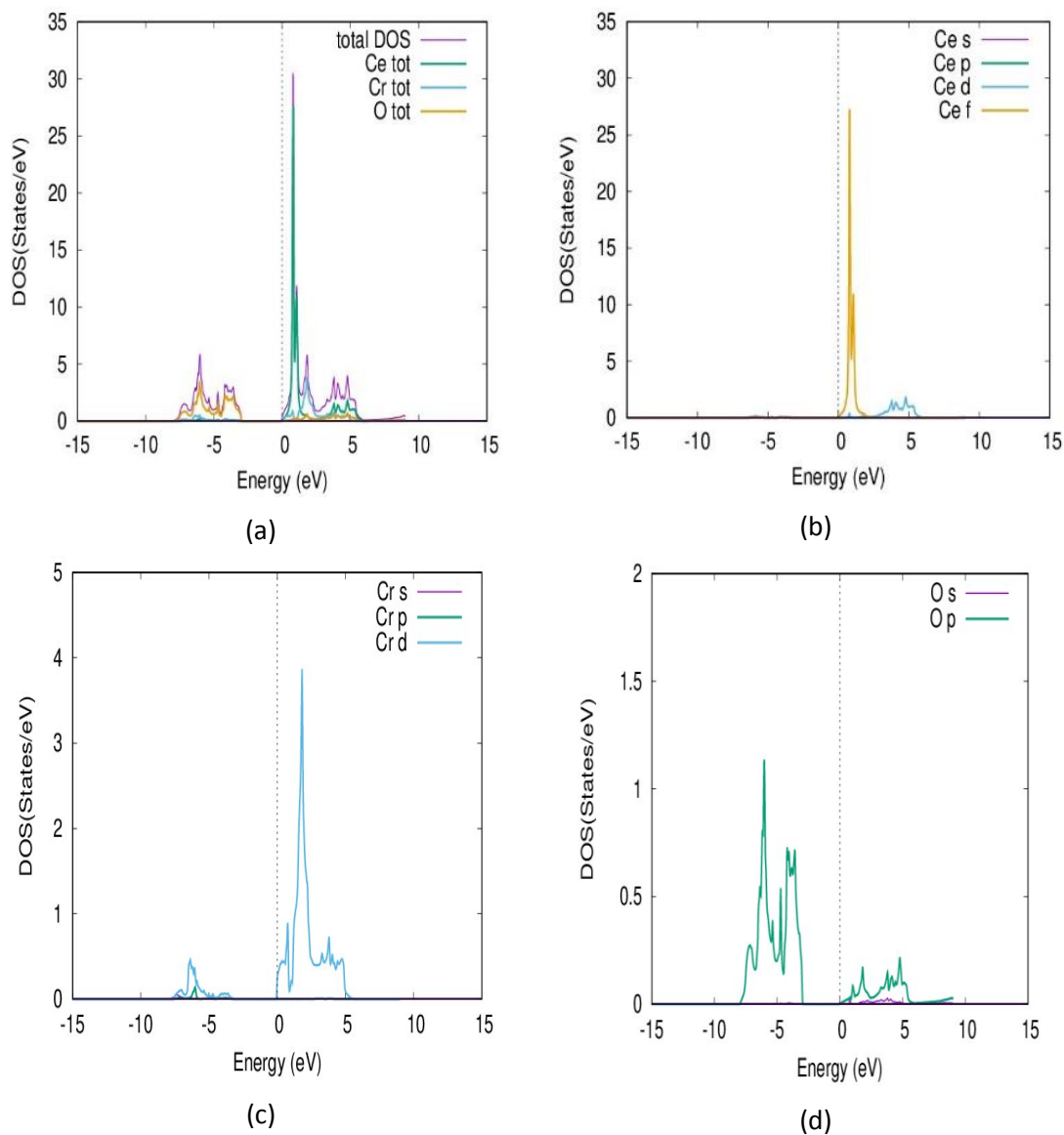


Figure. (20)

Total and partial density of state of spin up for (a) CeCrO_3 , (b) Ce, (c) Cr and (d) O of cubic CeCrO_3 compound with mBJ-GGA potential.

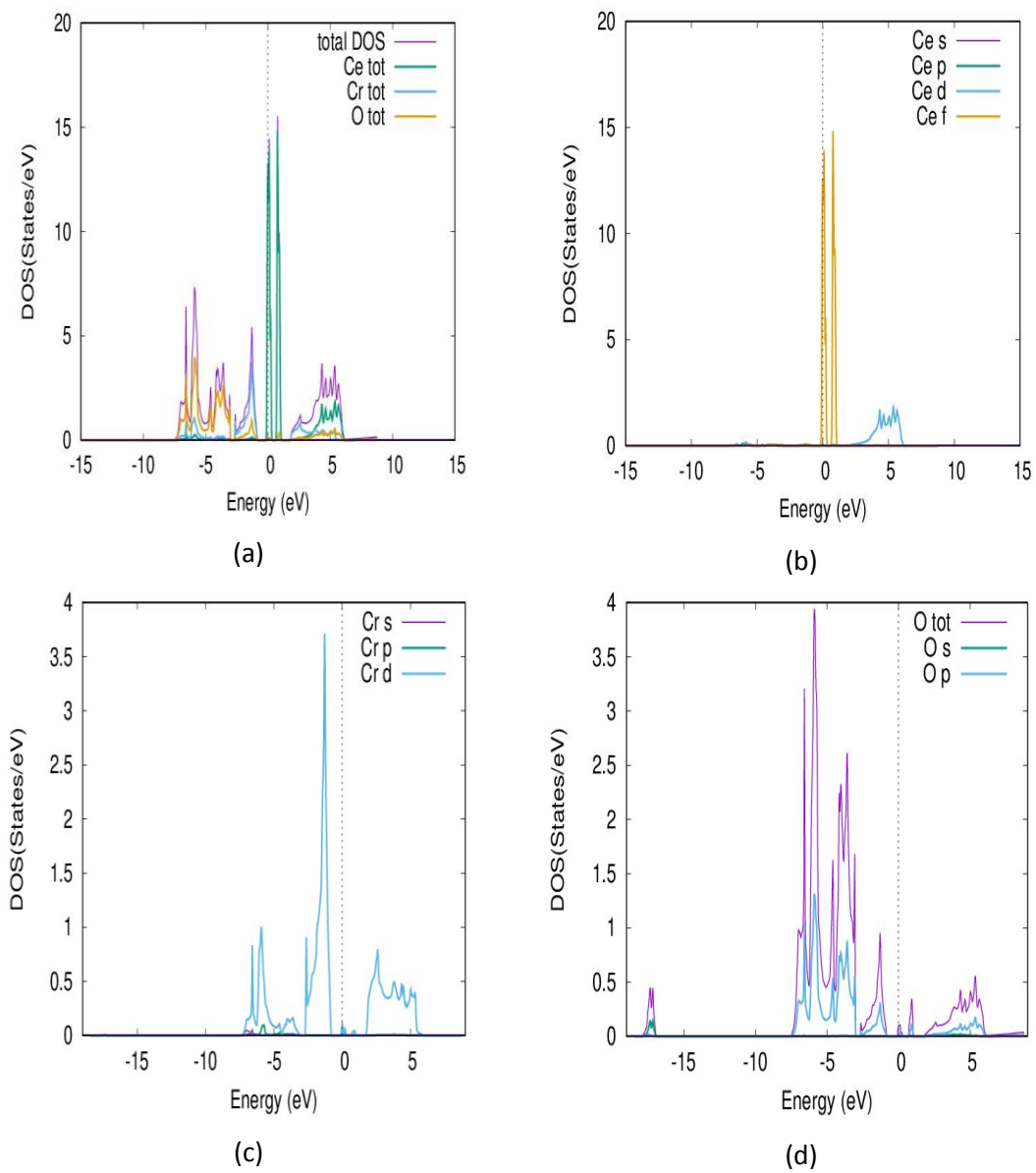


Figure. (21)

Total and partial density of state of spin down for (a) CeCrO_3 , (b) Ce, (c) Cr and (d) O of cubic CeCrO_3 compound with mBJ-GGA potential.

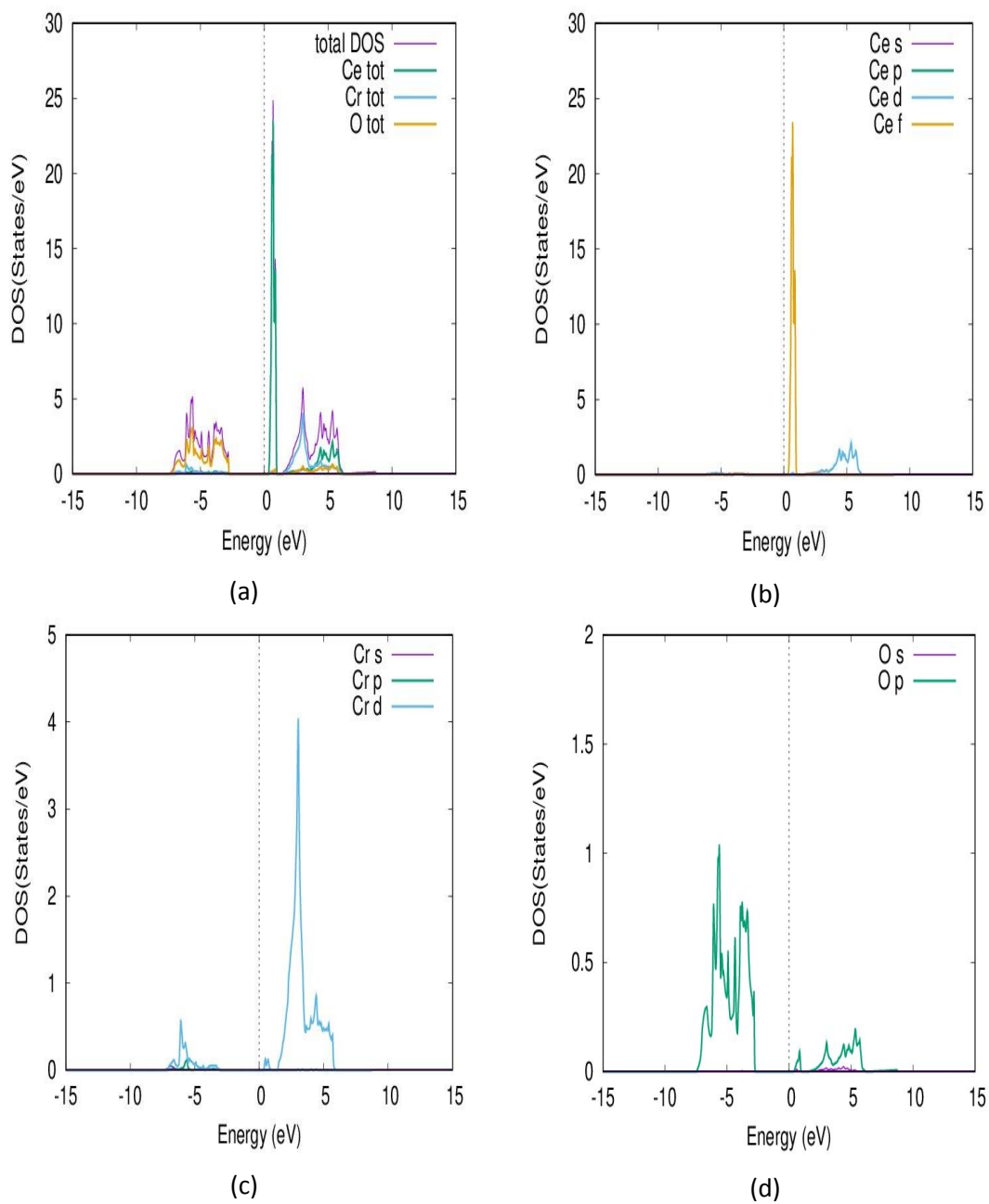


Figure. (22)

Total and partial density of state of spin up for (a) CeCrO_3 , (b) Ce, (c) Cr and (d) O of orthorhombic CeCrO_3 compound by using PBE-GGA.

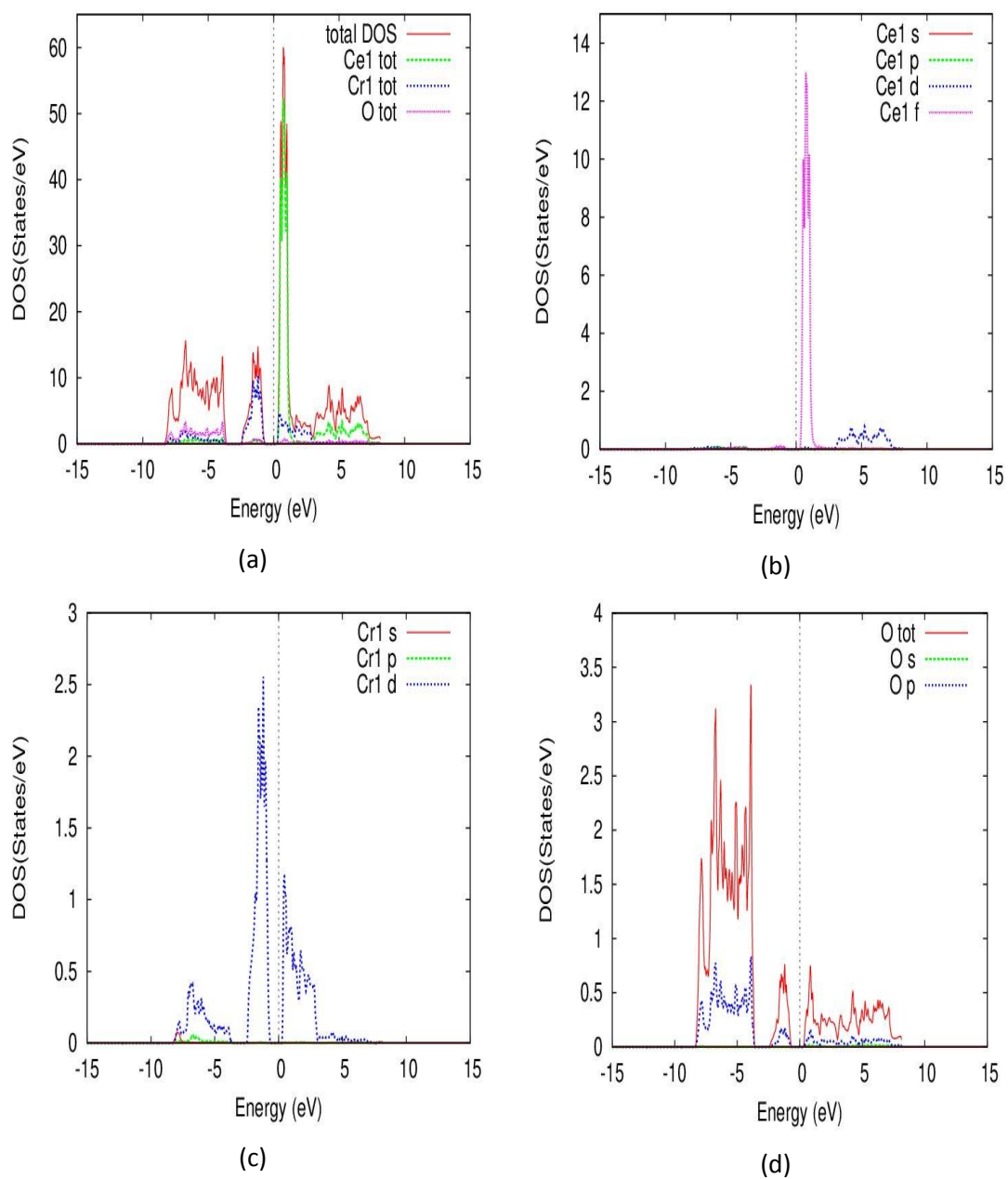


Figure. (23)

Total and partial density of state of spin down for (a) CeCrO_3 , (b) Ce, (c) Cr and (d) O of orthorhombic CeCrO_3 compound by using PBE-GGA.

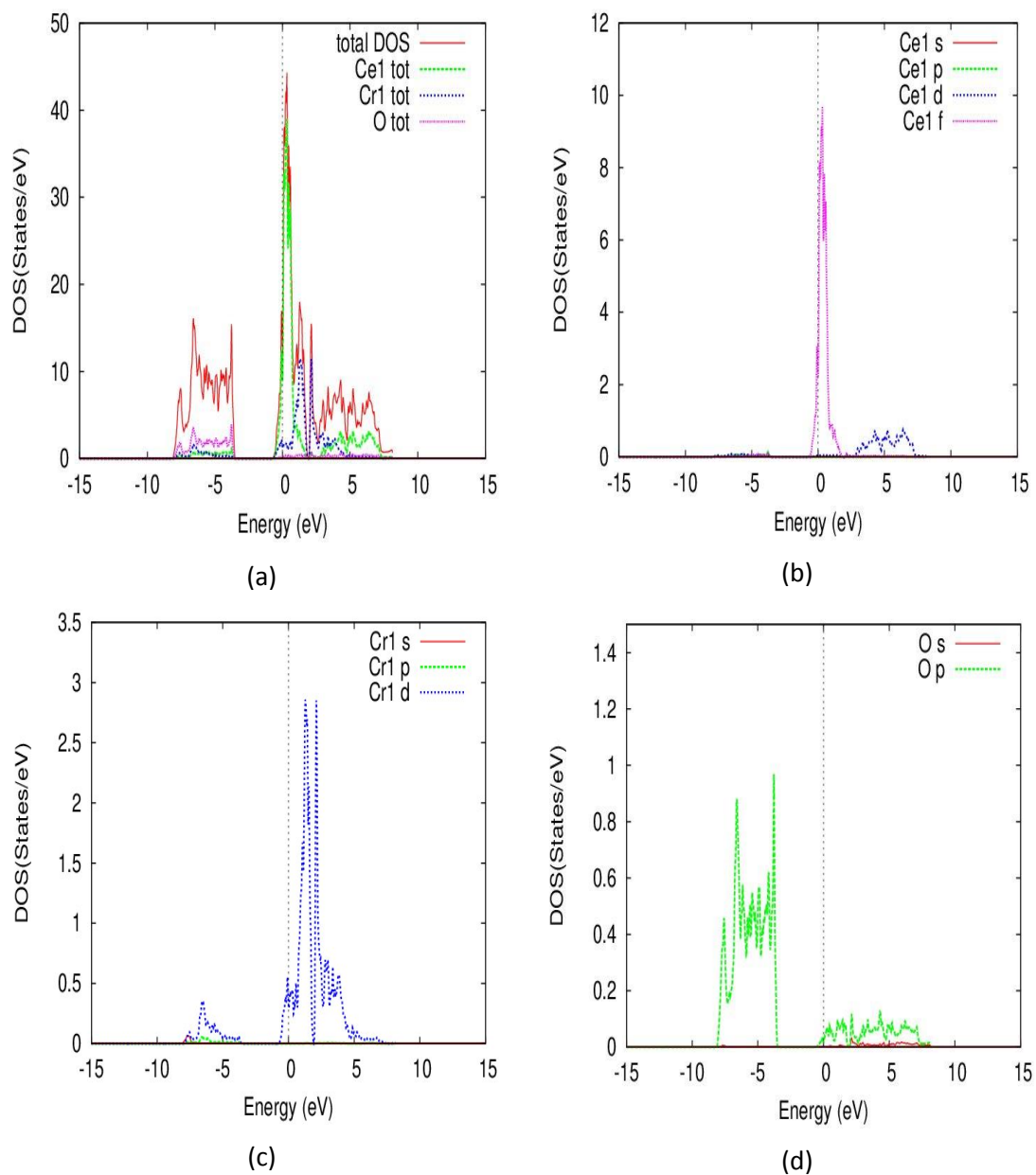


Figure. (24)

Total and partial density of state of spin up for (a) $CeCrO_3$, (b) Ce , (c) Cr and (d) O of orthorhombic $CeCrO_3$ compound with mBJ-GGA potential.

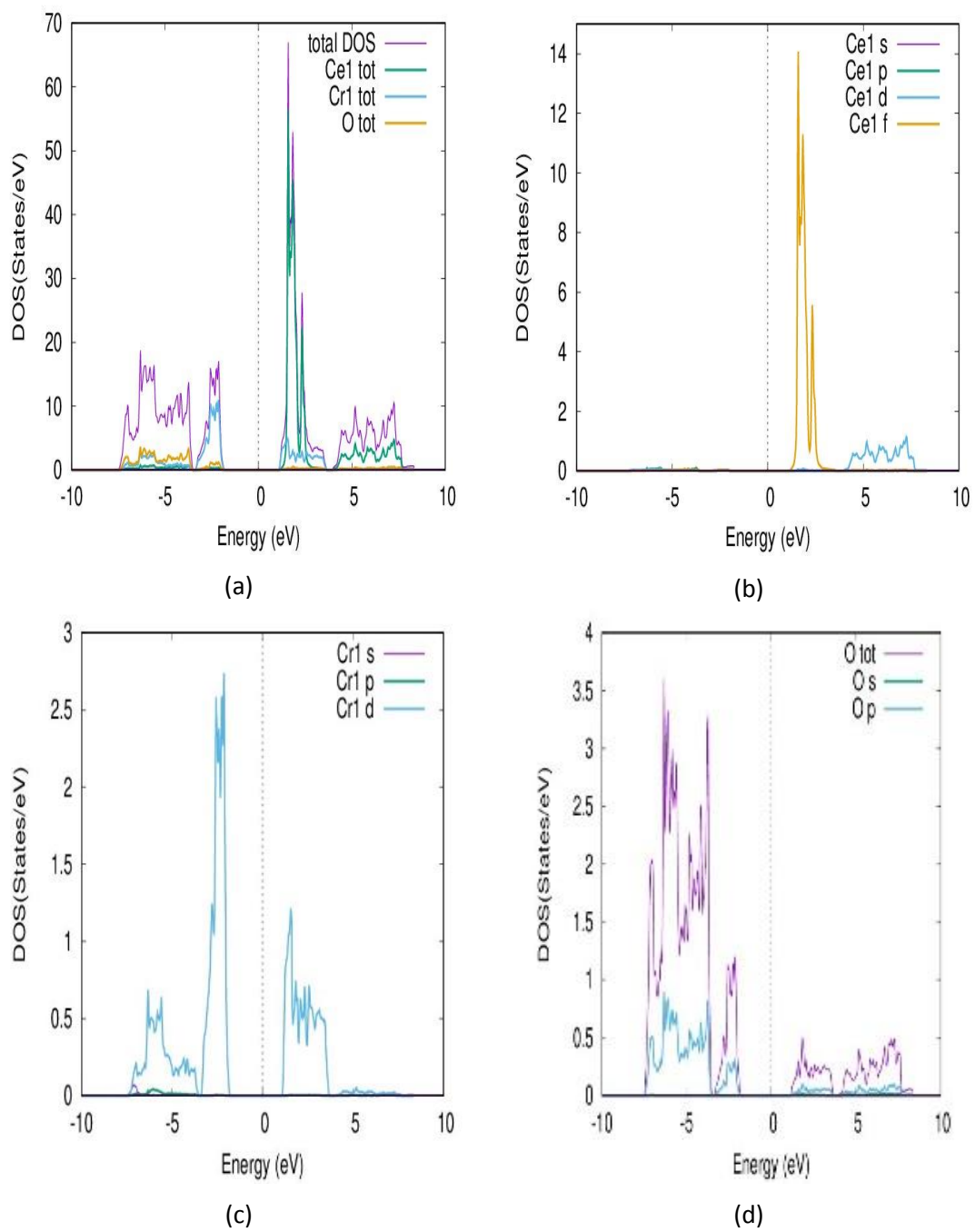


Figure. (25)

Total and partial density of state of spin down for (a) CeCrO_3 , (b) Ce, (c) Cr and (d) O of orthorhombic CeCrO_3 compound with mBJ-GGA potential.

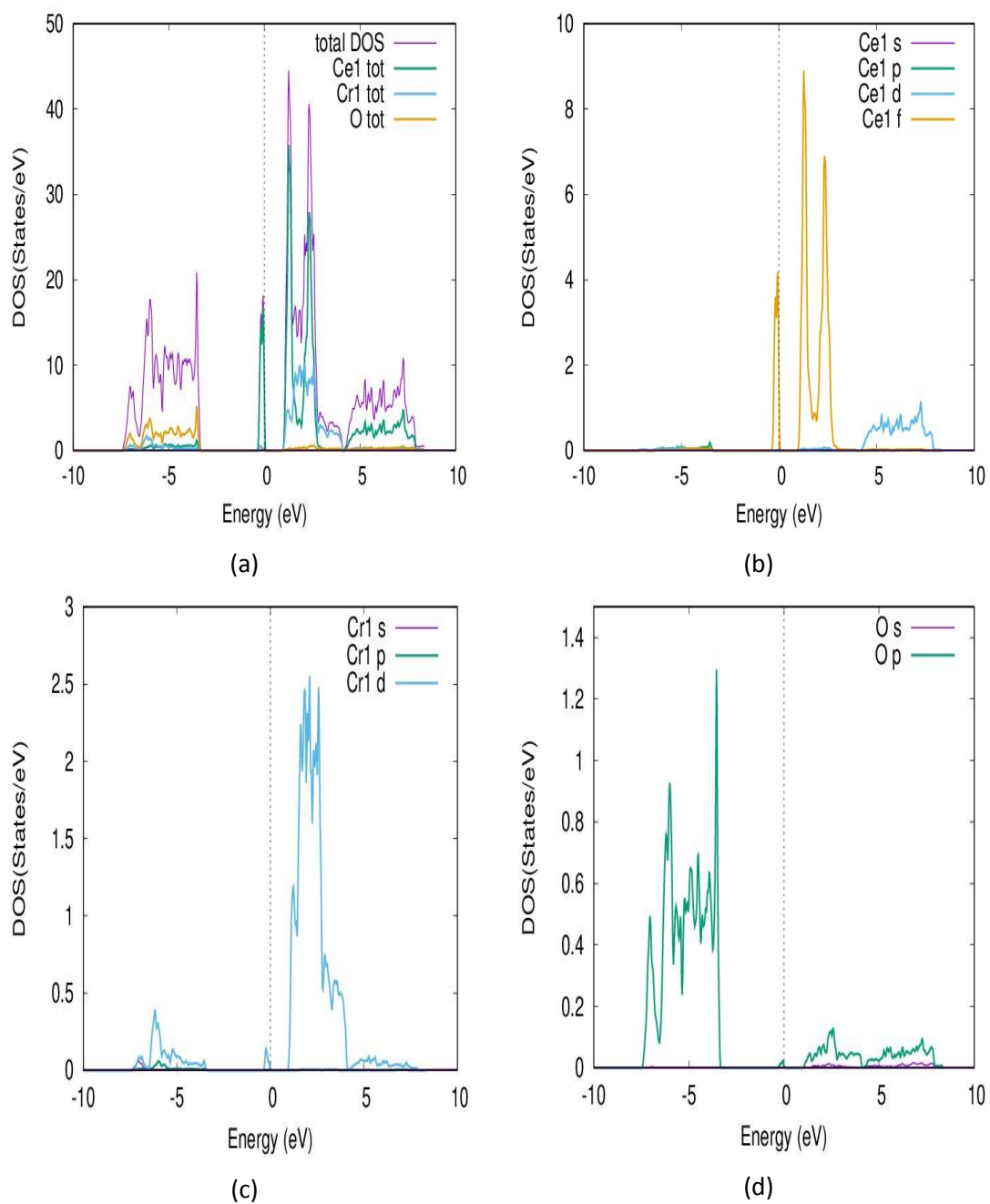


Figure. (26)

Total and partial density of state of spin up for (a) CeGaO_3 , (b) Ce, (c) Ga and (d) O of cubic CeGaO_3 compound by using PBE-GGA method.

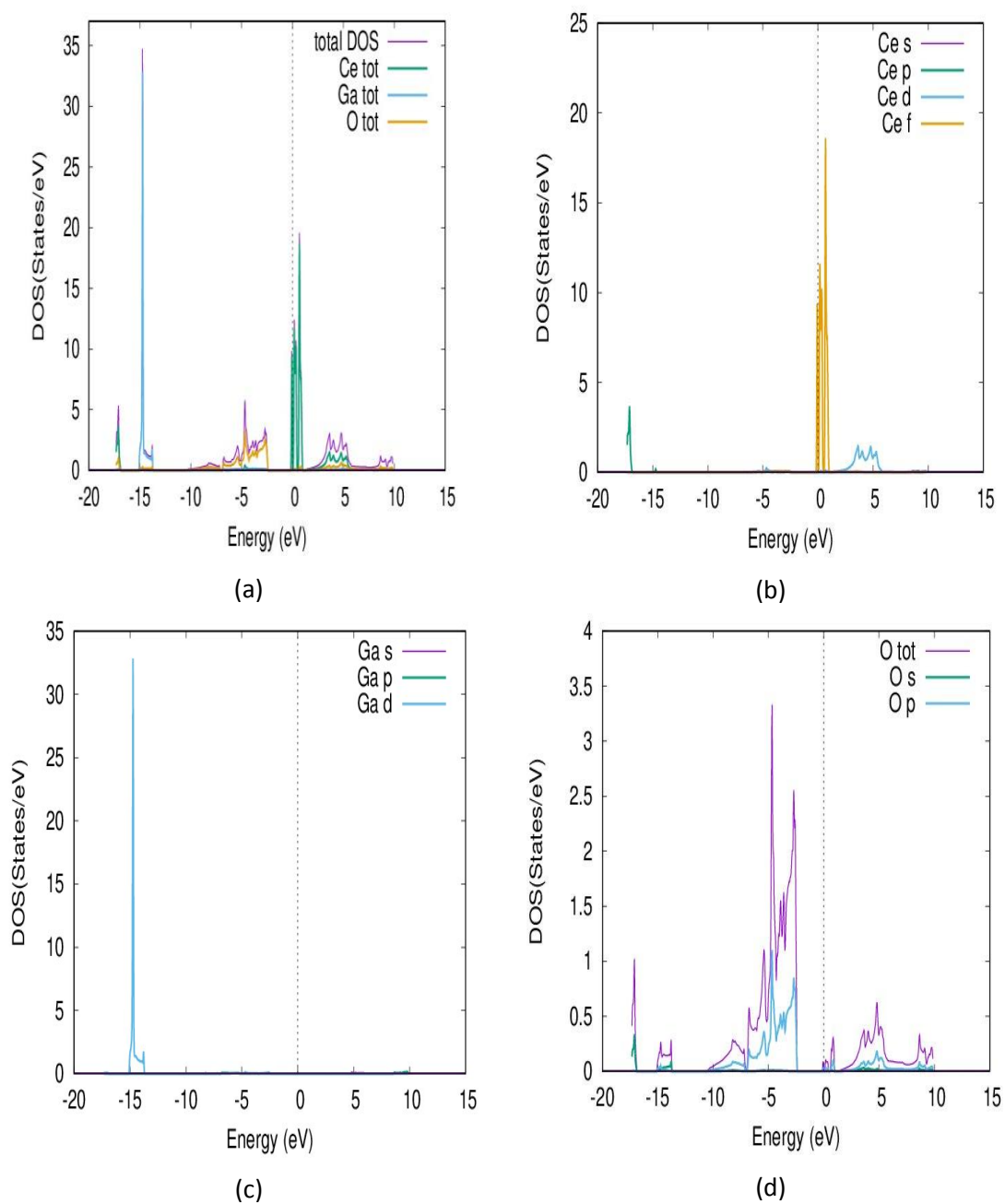


Figure. (27)

Total and partial density of state of spin down for (a) $CeGaO_3$, (b) Ce , (c) Ga and (d) O of cubic $CeGaO_3$ compound by using PBE-GGA method.

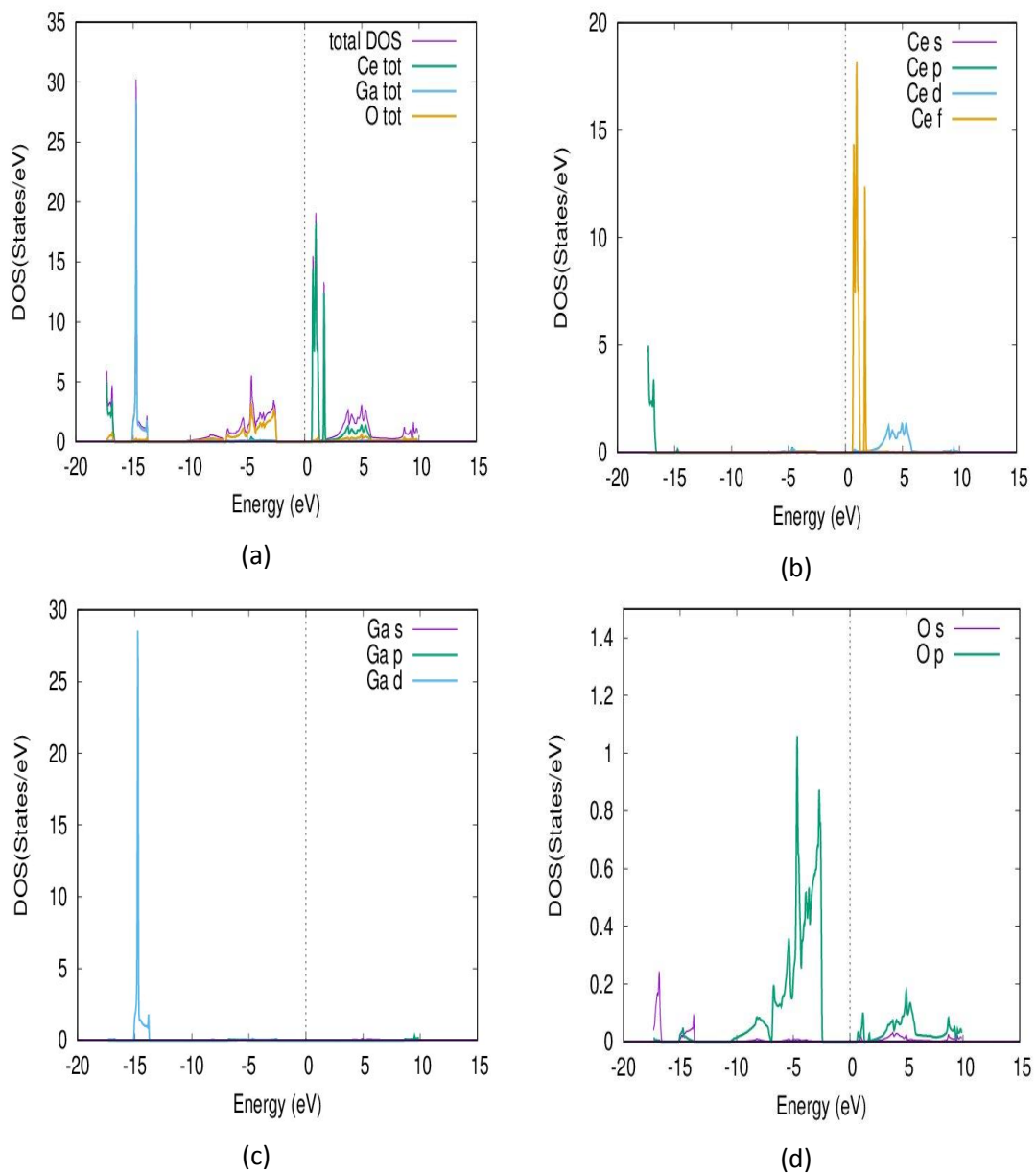


Figure. (28)

Total and partial density of state of spin up for (a) CeGaO_3 , (b) Ga, (c) Cr and (d) O of cubic CeGaO_3 compound with mBJ-GGA potential.

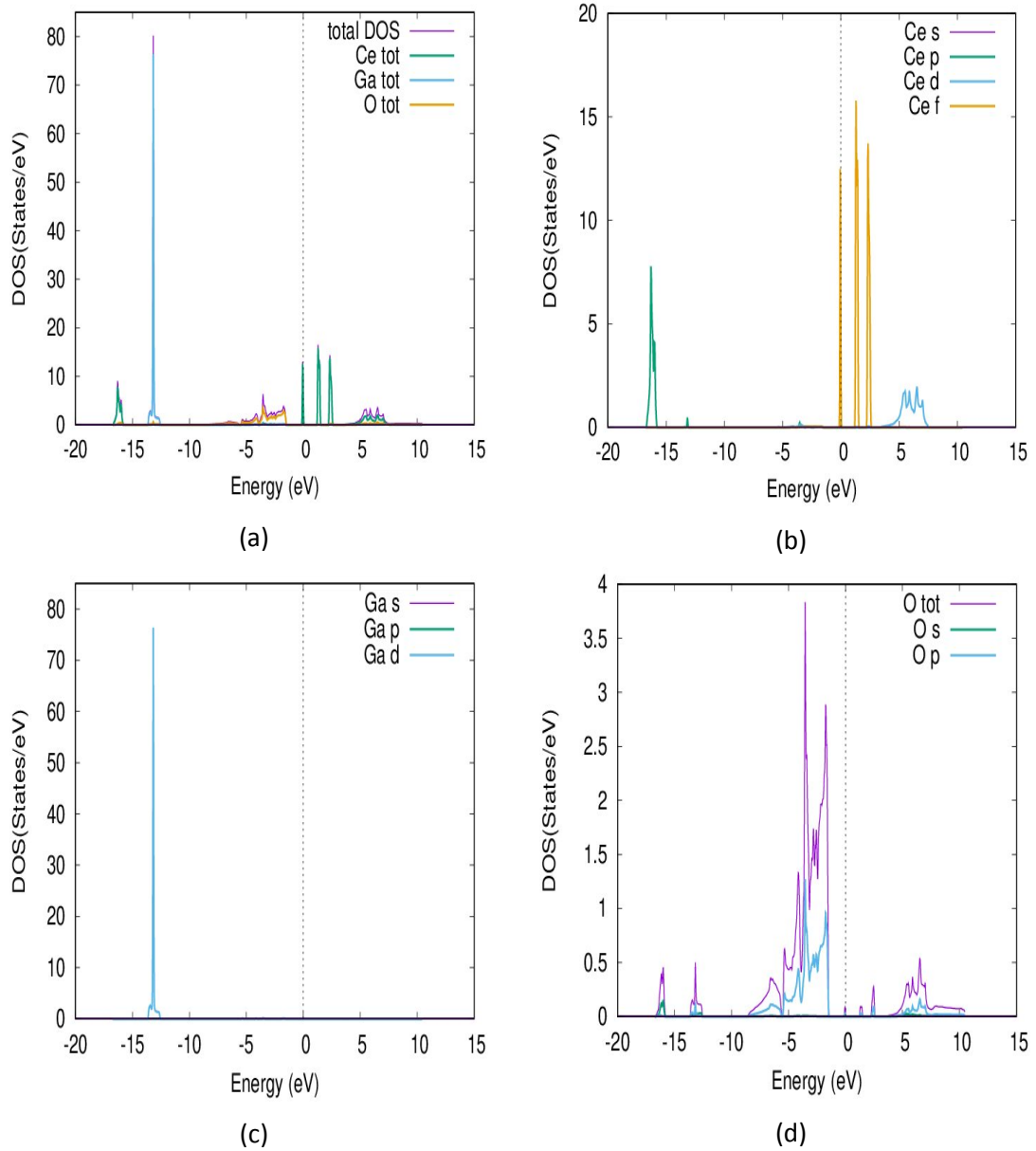


Figure. (29)

Total and partial density of state of spin down for (a) $CeGaO_3$, (b) Ga, (c) Cr and (d) O of cubic $CeGaO_3$ compound with mBJ-GGA potential.

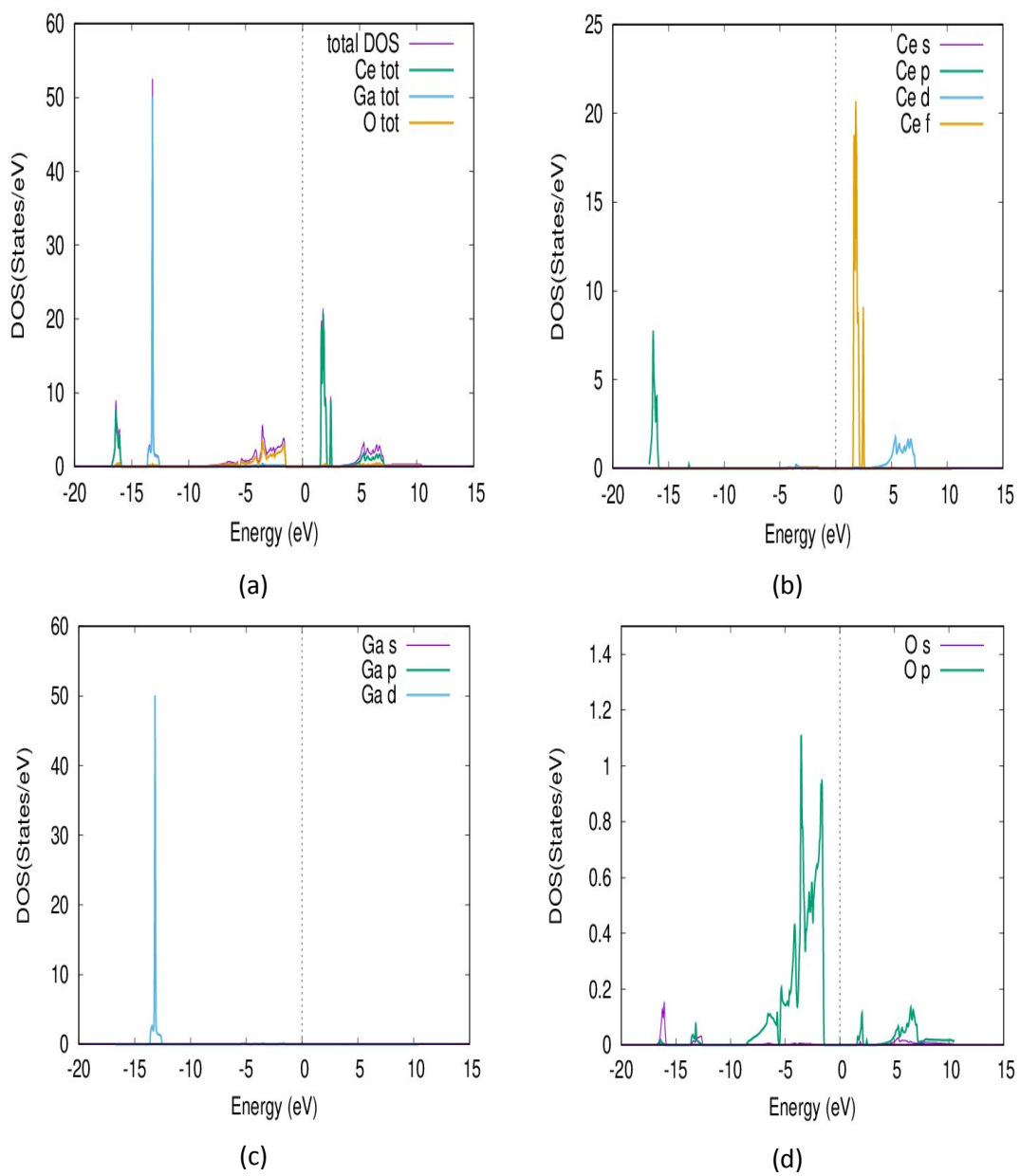


Figure (30)

Total and partial density of state of spin up for (a) $CeGaO_3$, (b) Ce, (c) Ga and (d) O of orthorhombic $CeGaO_3$ compound by using PBE-GGA.

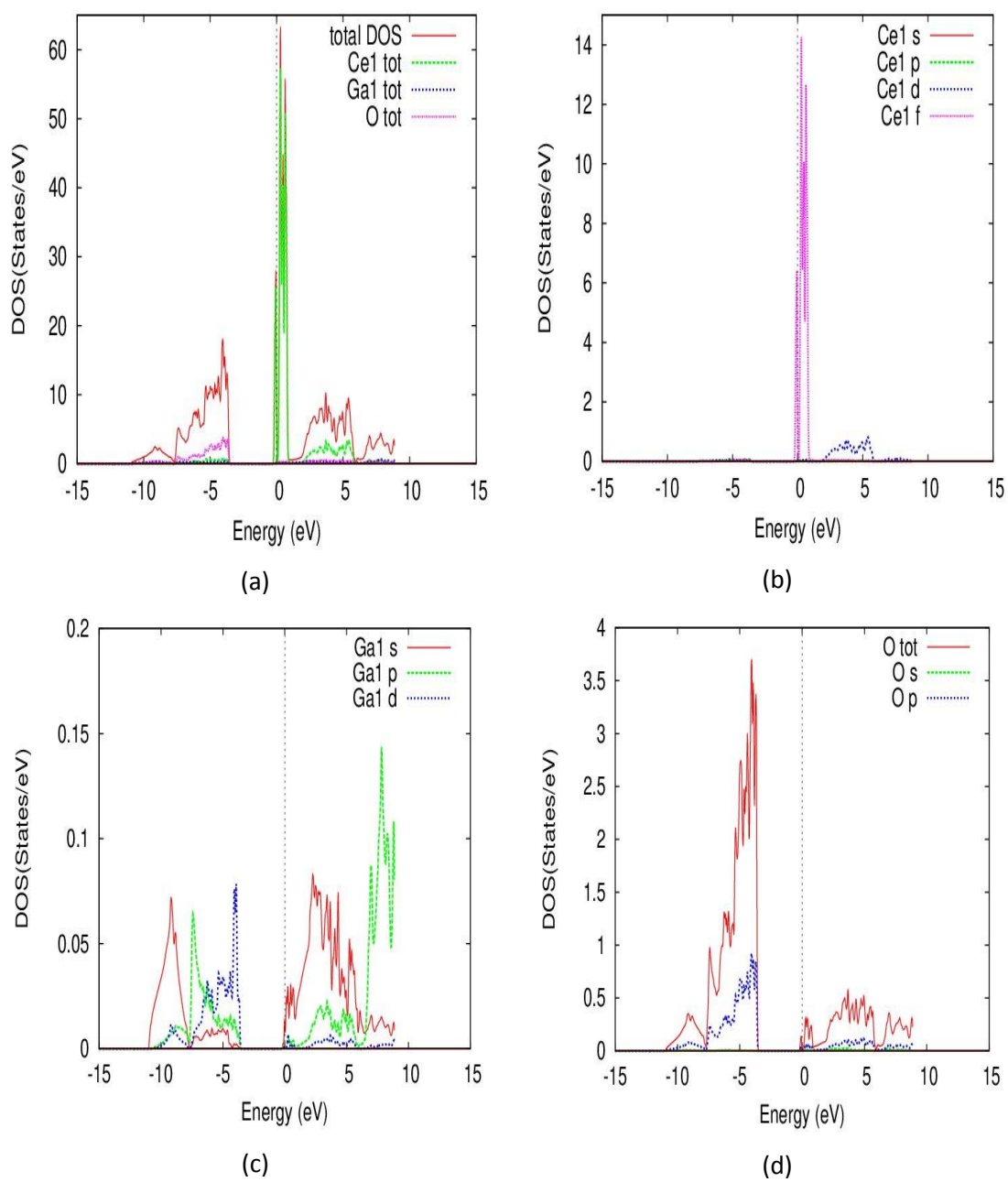


Figure (31)

Total and partial density of state of spin down for (a) $CeGaO_3$, (b) Ce , (c) Ga and (d) O of orthorhombic $CeGaO_3$ compound by using PBE-GGA.

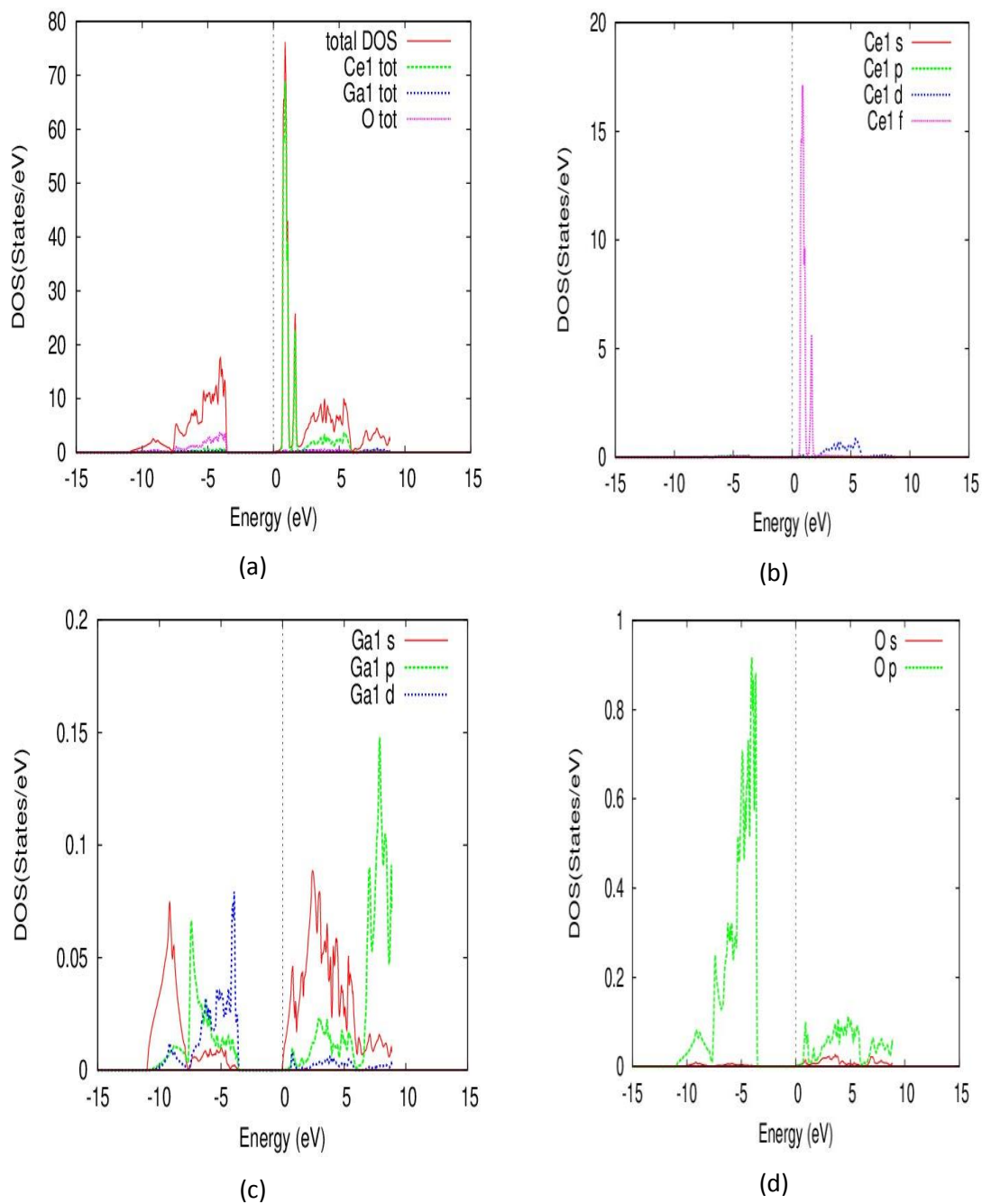


Figure (32)

Total and partial density of state of spin up for (a) $CeGaO_3$, (b) Ce , (c) Ga and (d) O of orthorhombic $CeGaO_3$ compound with mBJ-GGA potential.

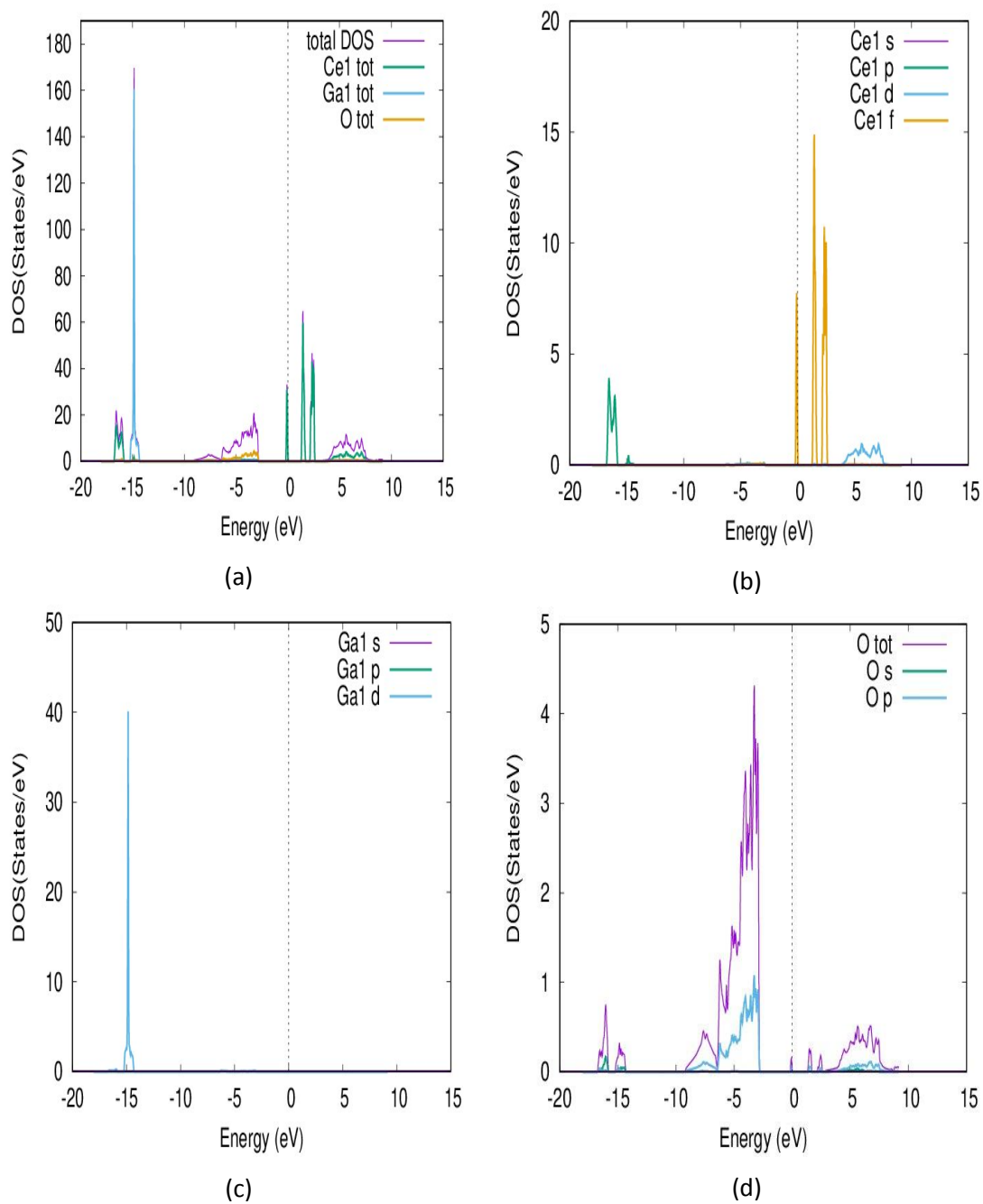
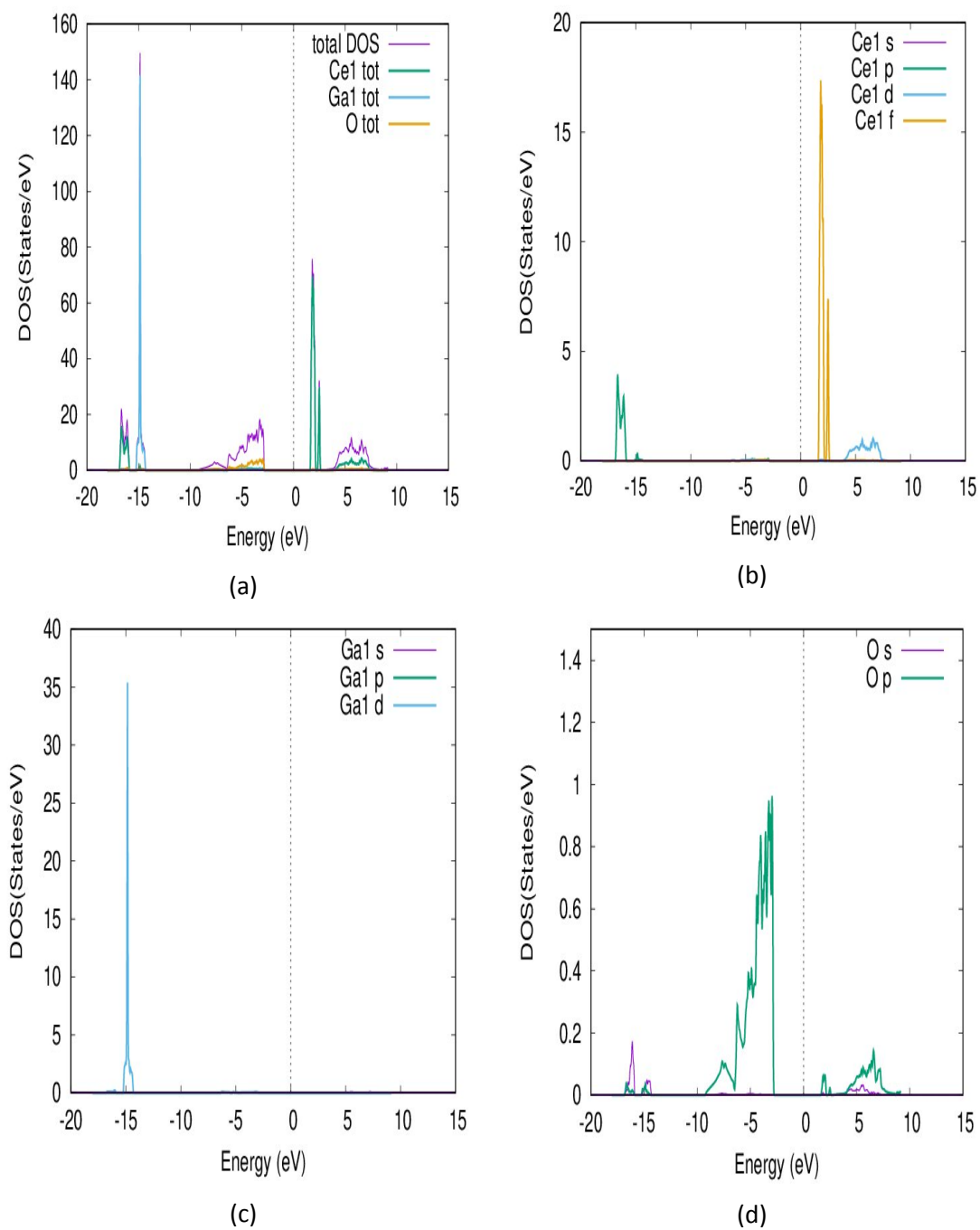


Figure (33)

Total and partial density of state of spin down for (a) CeGaO_3 , (b) Ce, (c) Ga and (d) O of orthorhombic CeGaO_3 compound with mBJ-GGA potential.





جامعة النجاح الوطنية

كلية الدراسات العليا

الخصائص التركيبية والالكترونية والمغناطيسية والمرونية للمركبات
 $CeCrO_3$, $CeGaO_3$ باستخدام طريقة الجهد التام

إعداد

عمر رستم مشرف كعبي

إشراف

أ. د. محمد أبو جعفر

د. محمود الفاروط

قدمت هذه الأطروحة استكمالاً لمتطلبات الحصول على درجة الماجستير في الفيزياء بكلية الدراسات العليا في
جامعة النجاح الوطنية في نابلس - فلسطين.

2022

الخصائص التركيبية والالكترونية والمغناطيسية والمرونية للمركبات $CeCrO_3$, $CeGaO_3$ باستخدام
طريقة الجهد التام

إعداد

عمر رستم مشرف كعبي

إشراف

أ. د. محمد أبو جعفر

د. محمود الفاروط

المخلص

تم فحص الخصائص التركيبية والالكترونية والمغناطيسية والمرونية لمركبات البيروفسكايت المكعب والمعيني القائم عن طريق استخدام جهد نظرية الكثافة الوظيفية (DFT) والجهد التام المزيد ذو الموجات المستوية الخطية (FP-LAPW) والتقريب التدريجي المعمم (PBE-GGA) بواسطة برنامج WIEN2k.

تم استخدام التقريب التدريجي المعمم (GGA) لحساب ثابت الشبكة (a) معامل الصلابة (B) ومشتقة معامل الصلابة بالنسبة للضغط (B') وقد تم استخدام نظام بيكي جونسون لتحسين فجوة الطاقة.

من أهم نتائج هذه الدراسة:

1. تبين أن المركب $CeCrO_3$ يمتلك خاصية نصف معدنية وأن المركب $CeGaO_3$ يمتلك خاصية

شبه موصل هذا في حالة المركبات مكعبة الشكل.

2. في حالة كان شكل المركبات معينية قائمة، تبين أن المركب $CeCrO_3$ يمتلك خاصية نصف معدنية

وأن المركب $CeGaO_3$ يمتلك خاصية شبه موصل في حالة المغزلي لأعلى أما في حالة المغزلي

لأسفل فهو عازل.

3. وجد أن المركبات $CeCrO_3$ و $CeGaO_3$ في كلا الشكلين المكعب والمعيني القائم لها خواص

مغناطيسية.

4. توافقت النتائج التي وجدناها بشكل كبير مع النتائج العملية والنظرية الأخرى.
5. من خلال الخواص المرورية تبين أن المركبات $CeCrO_3$ و $CeGaO_3$ في حالة الشكل مكعب لهما طبيعة مستقرة ميكانيكياً.
6. اتضح أن المركبات $CeCrO_3$ و $CeGaO_3$ في حالة الشكل مكعب لها روابط كيميائية أيونية.
7. تبين أن المركبات $CeCrO_3$ و $CeGaO_3$ في حالة الشكل مكعب قابلة للطرق والسحب.

الكلمات المفتاحية: البيروفسكايت المكعب، البيروفسكايت المعيني القائم، خاصية نصف معدنية، خصائص تركيبية، خصائص إلكترونية، خصائص مغناطيسية، خصائص مرورية.